COST ACTION TU1208

CIVIL ENGINEERING APPLICATIONS OF GROUND PENETRATING RADAR

Short-Term Scientific Missions & Training Schools

Year 1

Editors: Lara Pajewski & Marian Marciniak

EUROPEAN COOPERATION
IN SCIENCE AND TECHNOLOGY

TU1208 Basic Info
Start - End of Action: 4 April 2013 - 3 April 2017

Chair of the Action:
Dr. Lara Pajewski
Roma Tre University, IT
lara.pajewski@uniroma3.it

Vice-Chair of the Action:
Prof. Andreas Loizos
National Technical University of Athens, EL

COST TUD DC Chair:
Prof. Cristina Pronello
Politecnico di Torino, IT

COST TUD DC Rapporteur:
Dr. Goran Mladenovic
University of Belgrade, RS

COST Science Officer:
Dr. Mickael Pero
COST Office, BE

COST Administrative Officer:
Ms. Carmencita Malimban
COST Office, BE

Grant Holder:
Roma Tre University, Department of Engineering, IT

Editorial Coordinator of the Action:
Prof. Andrea Benedetto
Roma Tre University, IT

Chairs of Working Groups (WGs):
– WG1: Dr. Guido Manacorda, IDS Ingegneria dei Sistemi, IT
– WG2: Dr. Christina Plati, National Technical University of Athens, EL
– WG3: Dr. Antonis Giannopoulos, University of Edinburgh, UK
– WG4: Dr. Immo Trinks, Ludwig Boltzmann Institute for
  Archaeological Prospection and Virtual Archaeology, AT

Short-Term Scientific Missions (STSMs) Manager:
Prof. Marian Marciniak
National Institute of Telecommunications, PL
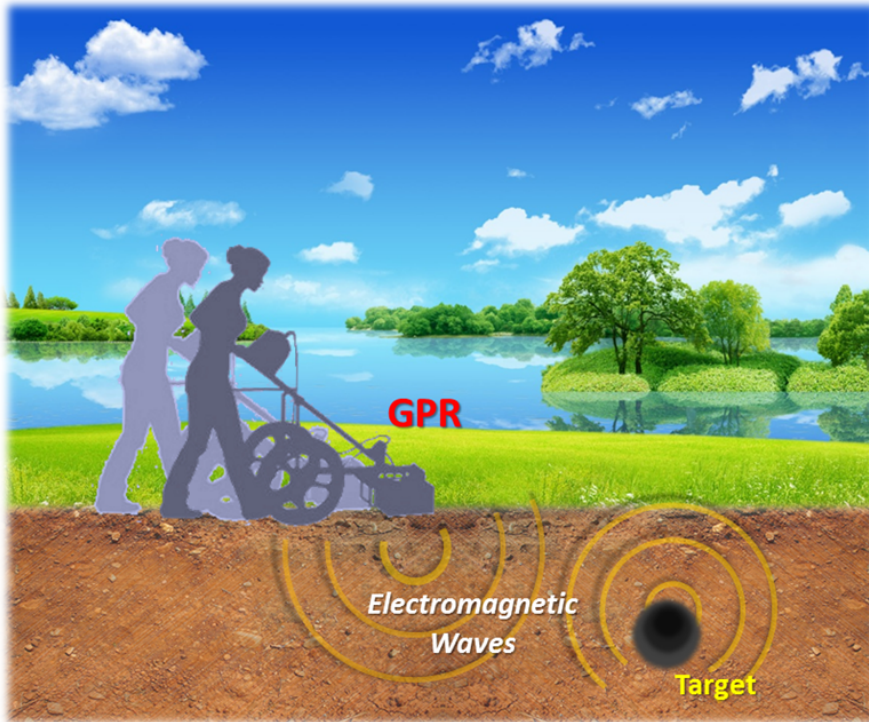
COST ACTION TU1208

CIVIL ENGINEERING APPLICATIONS OF GROUND PENETRATING RADAR

Short-Term Scientific Missions and Training Schools: Year 1
Editors: Lara Pajewski & Marian Marciniak

PREFACE
SHORT-TERM SCIENTIFIC MISSIONS AND TRAINING SCHOOLS: YEAR 1

COST ACTION TU1208
"CIVIL ENGINEERING APPLICATIONS OF GROUND PENETRATING RADAR"

Short-Term Scientific Missions (STSMs) and Training Schools (TSs) are among the most interesting networking tools supported by COST (European COoperation in Science and Technology). During Year 1 of the COST Action TU1208, four STSMs were funded and fruitfully carried out. Furthermore, two TSs were organised and successfully held. This book includes reports resuming these research and didactic activities.

STSMs are aimed at supporting individual mobility of European researchers, strengthening networks and fostering collaborations. They allow scientists to visit an institution or laboratory in a COST Country participating to the Action, or in an approved Near Neighbour Country (NNC) institution, or else in an approved International Partner Country (IPC) institution. STSMs shall specifically contribute to the scientific objectives of the Action offering the grant, at the same time allowing the visiting scientists to learn new techniques or gain access to specific instruments and/or methods not available in their own institutions.

STSM proposals have to be submitted by using the online application form, available at https://e-services.cost.eu/stsm. The Management Committee (MC) of the Action providing the grant performs their evaluation. The MC of the Action TU1208 formally delegated the evaluation of STSM applications to the Action Chair and STSM Manager. The selection of applicants is based on the scientific scope of the STSM application, which must be in line with the Action objectives, and on the applicant curriculum vitae. Geographical and gender balance issues are taken into consideration as well. STSM applicants must be engaged in a research programme as a postgraduate student or postdoctoral fellow, or be employed by or officially affiliated to an institution or

legal entity. This institution is considered as the Home institution. Institutions may be public or private entities.

Standard STSMs may have a minimum duration of 5 days and a maximum duration of 90 days. They need to be carried out in their entirety within a single grant period and within the Action's lifetime. Early-Stage Researchers (ESRs) may extend the duration of the STSM beyond the 90 days in well-justified cases (the maximum allowed duration is 180 days).

The participation of ESRs in STSMs is strongly encouraged. For COST, the definition of ESR is based on the time that elapses between the date of the PhD (or equivalent experience) and the date of involvement in a COST Action. If this time span is less than eight years, a person fits the definition; periods of career's leave have to be added to the mentioned time span. Supporting ESRs to develop independent careers and to establish their first research group under their own responsibility is a strategic priority for COST.

A STSM grant is a fixed financial contribution, based on the budget requested by the applicant and on the evaluation of the application by the MC Chair and STSM Manager. The aim of the grant is to support the costs associated with the exchange visit. It does not necessarily cover all expenses and has to be intended as a contribution to the travel and subsistence costs of the participant.

During Year 1 of the COST Action TU1208, 100% of the scientists who received STSM grants were ESRs or PhD Students and perfect gender balance was achieved. The list of funded STSMs is reported in the following:

A.
Granted ESR: Dr Lara Pajewski, IT - Host: Dr Antonis Giannopoulos, UK
STSM Title: *Electromagnetic modelling of Ground Penetrating Radar responses to complex targets*
Dates: from 21 October 2013 to 20 December 2013 - Location: University of Edinburgh, School of Engineering, Edinburgh, United Kingdom.

B.

Granted PhD Student: Philippe De Smedt, BE - Host: Dr Immo Trinks, AT

STSM Title: *Reconstructing prehistoric environments at Stonehenge with multiple electromagnetic survey methods*

Dates: from 1 February 2014 to 31 March 2014 - Location: Ludwig Boltzmann Institute for Archaeological Prospection and Virtual Archaeology, Vienna, Austria.

C.

Granted ESR: Dr Sonia Santos Assunçao, ES - Host: Klisthenis Dimitriadis, EL

STSM Title: *The preservation of the Tholos Tomb of Acharnon*

Dates: from 15 January 2014 to 15 February 2014 - Location: GEOSERVICE, Athens, Greece.

D.

Granted PhD Student: Iraklis Giannakis, UK – Host: Dr. Lara Pajewski, IT

STSM Title: *Numerical modelling of Ground-Penetrating Radar antennas*

Dates: from 15 January 2014 to 21 March 2014 - Location: Roma Tre University, Rome, Italy.

TSs aim at widening, broadening and sharing knowledge relevant to the Action's objectives, through the delivery of intensive training on a new and emerging subject. They can offer familiarisation with unique equipment or expertise that are typically to the benefit of ESR, although not exclusively.

COST financial support covers the organisation costs of TSs, as well as the participation of Trainees (by assigning grants) and Trainers (by reimbursing travel, accommodation and meal expenses). During Year 1 of the Action TU1208, 100% of the scientists who received TS Grants were ESRs or PhD Students, with a perfect gender balance among them.

The first TS organised by the COST Action TU1208 focused on "Microwave Imaging and Diagnostics: Theory, Techniques, Applications." It was held in Madonna di Campiglio, Italy, on March 24-28, 2014. It was a joint initiative of the Action TU1208, the Action TD1301 "Development of a European-based Collaborative Network to Accelerate Technological, Clinical and Commercialisation Progress in the Area of Medical Microwave Imaging," and the European School of Antennas (ESoA). Coordinators of the School were Prof Andrea Massa (IT) and Prof Tommaso Isernia (IT).

The second TS covered the state of the art and new trends on radar technologies: "Future Radar Systems: Radar2020." It was held in the Karlsruhe Institute of Technology, in Karlsruhe, Germany, on May 5-9, 2014. This course was co-organised by the Action TU1208, the ESoA, and the European Microwave Association (EuMA). The Coordinator was Prof Werner Wiesbeck (DE).

We are deeply grateful to COST, for funding the Action TU1208 "Civil Engineering Applications of Ground Penetrating Radar," the research and training activities presented here, and the publication of this book.

Lara Pajewski, Chair of the COST Action TU1208
Marian Marciniak, STSM Manager of the COST Action TU1208

STSM 1
ELECTROMAGNETIC MODELLING
OF GROUND PENETRATING RADAR RESPONSES TO COMPLEX TARGETS

Visiting ESR: Dr Lara Pajewski, "Roma Tre" University, Engineering Department, Rome, Italy (lara.pajewski@uniroma3.it)

Host: Prof Antonios Giannopoulos, The University of Edinburgh, School of Engineering, Edinburgh, United Kingdom

STSM Dates: 21 October 2013 – 20 December 2013

1. PURPOSE OF THE STSM

This STSM focused on the electromagnetic modelling of composite structures for Ground Penetrating Radar (GPR) applications, with the Finite-Difference Time-Domain (FDTD) technique. The main steps and achieved objectives of the STSM were:

1. Studying the FDTD technique and learning how to use the freeware tool GprMax, developed by Prof Antonios Giannopoulos.
2. Developing MATLAB procedures for the processing and visualization of GprMax output data. Such procedures are now available on the website of COST Action TU1208 for free public download.
3. Defining a set of test scenarios, to be used by research groups involved in the Working Group 3 of COST Action TU1208, to test and compare different electromagnetic forward- and inverse-scattering methods.
4. Modelling the test scenarios defined in 3 with GprMax.

An additional objective of the STSM was that of interacting with the Chair of COST Action TU1206, Dr Seumas Campbell, British Geological Survey, Edinburgh, United Kingdom, in order to find out topics of common interest and possible synergies between Actions TU1206 and TU1208.

2. DESCRIPTION OF THE WORK CARRIED OUT DURING THE STSM AND OF THE MAIN RESULTS OBTAINED

2.1: THE FDTD TECHNIQUE AND GprMax

In order to predict correctly the GPR response from a particular scenario, Maxwell's equations have to be solved, subject to the physical and geometrical properties of the considered problem and to its initial conditions. Several techniques have been developed in computational electromagnetics, for the solution of Maxwell's equations. These methods can be classified into two main categories: differential and integral equation solvers, which can be implemented in the time or frequency domain. The differential solvers include the FDTD and Finite-Volume Time-Domain (FVTD) techniques, the Finite Element Method (FEM) and Transmission Line Method (TLM). The Method of Moments (MoM), instead, is an integral equation method. All of the different techniques present compromises between computational efficiency, stability, and the ability to model complex geometries. The FDTD presents several advantages: it has inherent simplicity, efficiency and conditional stability; it is highly versatile; it has become a mature and well-researched technique.

GprMax [1] is a well-known and largely validated FDTD simulator, developed by Prof. Antonios Giannopoulos and available for free public download on www.GprMax.com, along with a detailed user guide.

The first part of the STSM was devoted to studying the FDTD technique and to learning how to use GprMax. There is a very large amount of information on the FDTD available in the literature; good starting points are [2]-[4], whereas the specific application of FDTD to the GPR forward scattering problem is described in [5]. The GprMax user guide describes the installation of GprMax2D and GprMax3D simulators and the various commands which are available for the construction of 2D and 3D GPR models; it provides some examples, to illustrate the procedures that should be followed in order to obtain useful

models employing GprMax2D/3D; it includes useful hints and tips, explaining the most fundamental aspects of using an FDTD-based program and how to avoid the most common errors.

<div align="center">

2.2: MATLAB PROCEDURES
FOR THE PROCESSING AND VISUALIZATION OF GPRMAX OUTPUT DATA

</div>

On the GprMax website, some MATLAB functions are available for free download: they can be used to import in MATLAB the GprMax2D/3D output data, stored in binary format, in order to process and visualize them.

The second part of the STSM was devoted to the development of further MATLAB procedures. These procedures are very simple, however it is believed that scientists willing to use GprMax will find them useful (especially those who aren't expert users of MATLAB). They are available for free public download on the COST Action TU1208 website www.GPRadar.eu. They are reported and shortly described in the following.

2.2.1: ascan2D.m

This procedure can be used to plot an A-scan, generated by GprMax2D. Here and in the following, according to a nomenclature widely accepted by the GPR community, the term 'A-scan' refers to an array of electric-field values calculated in a fixed spatial point and in T consecutive instants (a GPR trace).

```
% ------ascan2D------
%
% This Matlab procedure uses data generated by 'GprMax2D',
% electromagnetic wave simulator for Ground Penetrating Radar (GPR) modelling,
% in order to display an A-scan at a given trace-number.
%
% An A-scan is a single waveform recorded by the GPR, where the receiver is in a fixed
% position and, therefore, the only variable is the time, which is related to the
% survey's depth by the propagation velocity.
%
% European Cooperation in Science and Technology (COST)
% COST Action TU1208 "Civil Engineering Applications of Ground Penetrating Radar"
```

```
% 2013 - 2017, www.GPRadar.eu, Chair: Lara Pajewski, Italy
clear all;
name = 'filename.out';      % 'filename.out' is the output file generated by 'GprMax2D'
[Header, Fields] = GprMax( name )
E(:,:) = Fields.ez(:,1,:);     % extracts the values of the Ez component
tw=Fields.t*10^9;            % extracts the vector of time instants, in ns
figure;
tracenum=1;                  % you can put here the number of the A-scan to be plotted
plot(tw,E(:,tracenum),'LineWidth',2)
title('A-scan','fontsize',20);
ylabel('Amplitude','fontsize',18);
xlabel('Time [ns]','fontsize',18);
legend('Trace');
```

2.2.2: ascan3D.m

This procedure can be used to plot an A-scan, generated by GprMax3D.

```
% ------ascan3D------
%
% This Matlab procedure uses data generated by 'GprMax3D',
% electromagnetic wave simulator for Ground Penetrating Radar (GPR) modelling,
% in order to display an A-scan at a given trace-number.
%
% An A-scan is a single waveform recorded by the GPR, where the receiver is in a fixed
% position and, therefore, the only variable is the time, which is related to the
% survey's depth by the propagation velocity.
%
% European Cooperation in Science and Technology (COST)
% COST Action TU1208 "Civil Engineering Applications of Ground Penetrating Radar"
% 2013 - 2017, www.GPRadar.eu, Chair: Lara Pajewski, Italy

clear all
name = 'filename.out';                  % 'filename.out' is the file generated by 'GprMax3D'
[Header, Fields] = GprMax( name ); % extracts the E-field components
Ex = Fields.ex(:,:);
Ey = Fields.ey(:,:);
Ez = Fields.ez(:,:);
tw=Fields.t*10^9;      % extracts the vector of time instants, in ns
figure;
tracenum=1;           % you can put here the number of the A-scan to be plotted
plot(tw,Ex(:,tracenum),tw,Ey(:,tracenum), 'r',tw,Ez(:,tracenum),'g','LineWidth',2)
title('A-scan','fontsize',18);
ylabel('Amplitude','fontsize',14);
xlabel('Time [ns]','fontsize',14); legend('Ex','Ey','Ez');
```

10

2.2.3: ascan2Dback.m

This procedure can be used to plot an A-scan of the back-scattered field, generated by GprMax2D. In order to obtain the field back-scattered by an object (or by a set of objects), according to the electromagnetic-field superposition principle valid for all linear systems, GprMax2D has to be run twice: a first time, it has to be run in the presence of the complete scenario; a second time, it has to be run in the presence of the same scenario without the scattering object (or set of objects). The difference between the obtained results will give the back-scattered field.

```
% ------ascan2Dback------
%
% This Matlab procedure uses data generated by 'GprMax2D',
% electromagnetic wave simulator for Ground Penetrating Radar (GPR) modelling,
% in order to display an A-scan of the Back-Scattered Field at a given trace-number.
%
% An A-scan of the Back-Scattered Field is obtained by subtracting
% the undisturbed A-scan (i.e. without scatterers) from the one with scatterers.
%
% European Cooperation in Science and Technology (COST)
% COST Action TU1208 "Civil Engineering Applications of Ground Penetrating Radar"
% 2013 - 2017, www.GPRadar.eu, Chair: Lara Pajewski, Italy

clear all;
%   name = 'filename.out', where filename is the name of file generated by 'GprMax2D'
name1 = 'filename1.out';          %    undisturbed A-scan
name2 = 'filename2.out';          %    A-scan with scatterers
[Header, Fields] = GprMax( name1 )
E1(:,:) = Fields.ez(:,1,:);
[Header, Fields] = GprMax( name2 );
E2(:,:) = Fields.ez(:,1,:);
E = E2-E1;                % subtracts the undisturbed A-scan from the one with scatterers
tw=Fields.t*10^9;        % extracts the vector of time instants, in ns
figure;
tracenum=1;              % you can put here the number of the A-scan to be plotted
plot(tw,E(:,tracenum),'LineWidth',2)
title('A-scan of the Back-Scattered Field','fontsize',20);
ylabel('Amplitude','fontsize',18);
xlabel('Time [ns]','fontsize',18);
legend('Trace');
```

11

2.2.4: `bscan2D.m`

This procedure can be used to plot a B-scan, generated by GprMax2D. Here and in the following, the term 'B-scan' corresponds to a matrix of electric-field values, calculated in T time instants and M different spatial points, meaning M A-scans (this is equivalent to assuming that a GPR 'stops' in M positions, for example along a line parallel to the air-soil interface, gathering data in each of them; the B-scan is the comprehensive set of GPR traces).

```
% ------bscan2D------
%
% This Matlab procedure uses data generated by 'GprMax2D',
% electromagnetic wave simulator for Ground Penetrating Radar (GPR) modelling,
% in order to display a B-scan.
%
% A B-scan is a set of A-scans, obtained by moving the transmitter and receiver
% of the GPR on a line (e.g. x-axis), thus creating a 2D dataset,
% the amplitude of the received signal is usually plotted in a grey-scale map
% or in contour plots. The output of this procedure is a grey-scale map.
%
% European Cooperation in Science and Technology (COST)
% COST Action TU1208 "Civil Engineering Applications of Ground Penetrating Radar"
% 2013 - 2017, www.GPRadar.eu, Chair: Lara Pajewski, Italy

clear all;
% name = 'filename.out', where filename is the name of file generated by 'GprMax2D'
name = 'filename.out';
[Header, Fields] = GprMax( name )  % extracts the values of the field component Ez
E(:,:) = Fields.ez(:,1,:);
tw=Fields.t*10^9;                   % extracts the vector of time instants, in ns
% a vector relative to the receiver-position is now created
    for j=1:Header.NSteps
    rxposition(j)=Header.rx*Header.dx+Header.RxStepX*(j-1)*Header.dx;
    end
figure;
imagesc(rxposition,tw,E);
colormap gray;
title('B-scan','fontsize',20);
colorbar ('location', 'eastoutside');
ylabel('Time [ns]','fontsize',18);
xlabel('Receiver-position [m]','fontsize',18);
```

12

2.2.5: `bscan3D.m`

This procedure can be used to plot a B-scan, generated by GprMax3D.

```
% ------bscan3D------
%
% This Matlab procedure uses data generated by 'GprMax3D',
% electromagnetic wave simulator for Ground Penetrating Radar (GPR) modelling,
% in order to display a B-scan.
%
% A B-scan is a set of A-scans, obtained by moving the transmitter and receiver
% of the GPR on a line (e.g. x-axis), thus creating a 2D dataset;
% the amplitude of the received signal is usually plotted in a grey-scale map.
%
% European Cooperation in Science and Technology (COST)
% COST Action TU1208 "Civil Engineering Applications of Ground Penetrating Radar"
% 2013 - 2017, www.GPRadar.eu, Chair: Lara Pajewski

clear all;
name = 'filename.out';  % filename is the name of file generated by 'GprMax3D'
[Header, Fields] = GprMax( name )
%extract the values of all three components of the field E
Ex = Fields.ex(:,:); Ey = Fields.ey(:,:); Ez = Fields.ez(:,:);E = Ex+Ey+Ez;
tw=Fields.t*10^9; %extract the vector of time instants, in ns
%create vectors relative to the size of the model's domain
    for j=1:Header.NSteps
    X(j)=Header.rx*Header.dx+Header.RxStepX*(j-1)*Header.dx;
    Y(j)=Header.ry*Header.dy+Header.RxStepY*(j-1)*Header.dy;
    Z(j)=Header.rz*Header.dz+Header.RxStepZ*(j-1)*Header.dz;
    end
figure;
imagesc(Y,tw,Ex);
colormap gray
title('B-scan','fontsize',20); colorbar
ylabel('Time [ns]','fontsize',18);
xlabel('Receiver-position [m]','fontsize',18);
```

2.2.6: `bscan2Dback.m`

This procedure can be used to plot a B-scan of the back-scattered field, generated by GprMax2D.

```
% ------bscan2Dback------
%
% This Matlab procedure uses data generated by 'GprMax2D',
```

```
% electromagnetic wave simulator for Ground Penetrating Radar (GPR) modelling,
% in order to display a B-scan of the Back-Scattered Field.
%
% A B-scan of the Back-Scattered Field is obtained by subtracting
% the undisturbed B-scan (i.e. without scatterers) from the one with scatterers.
%
% European Cooperation in Science and Technology (COST)
% COST Action TU1208 "Civil Engineering Applications of Ground Penetrating Radar"
% 2013 - 2017, www.GPRadar.eu, Chair: Lara Pajewski, Italy

clear all;
name1 = '.out'; %undisturbed B-scan
name2 = '.out'; %B-scan with scatterers
[Header, Fields] = GprMax( name1 )
E1(:,:) = Fields.ez(:,1,:);
[Header, Fields] = GprMax( name2 );
E2(:,:) = Fields.ez(:,1,:);
E = E2-E1;   % subtracts the undisturbed B-scan from the one with scatterers
% creates a vector with the receiver-positions
   for j=1:Header.NSteps
   rxposition(j)=Header.rx*Header.dx+Header.RxStepX*(j-1)*Header.dx;
   end
tw=Fields.t*10^9;        % extracts the vector of time instants, in ns
figure;
imagesc(rxposition,tw,E);
colormap gray
title('B-scan of the Back-Scattered Field','fontsize',20);
colorbar ('location', 'eastoutside');
ylabel('Time [ns]','fontsize',18);
xlabel('Receiver-position [m]','fontsize',18);
```

2.2.7: geo2D.m

This procedure can be used to display the geometry of the model, generated by GprMax2D.

```
%------geo2D------
%
% This Matlab procedure uses data generated by 'GprMax2D',
% electromagnetic wave simulator for Ground Penetrating Radar (GPR) modelling,
% in order to display the geometry of the model.
%
% European Cooperation in Science and Technology (COST)
% COST Action TU1208 "Civil Engineering Applications of Ground Penetrating Radar"
% 2013 - 2017, www.GPRadar.eu, Chair: Lara Pajewski, Italy

clear all;
% name = 'filename.geo', where filename is the name of file generated by 'GprMax2D'
```

```
name = 'filename.geo';
[mesh,header,media] = GprMax2g(name)
% extracts the model's geometry data through the function GprMax2g
C(:,:) = mesh(:,:);
% create vectors relative to the size of the model's domain
X=(0:header.nx) * header.dx;
Y=(0:header.ny) * header.dy;
figure; imagesc(X,Y,C);
xlabel('[m]','fontsize',18);
ylabel('[m]','fontsize',18);
% By default, imagesc plots the y-axis from lowest to highest value, top to bottom.
% To reverse this, type set(gca,'YDir','normal').
% This will reverse both the y-axis and the image.
set(gca,'YDir','normal');
axis image;
N = media.num
% specify here the number of different media defined in the model
colours=gray(N);
%  colormap(colours)
colormap(flipud(colours));
% flips/inverts the colours of the colormap
hold on;
%  the legend is now defined
L = line(ones(N),ones(N), 'LineWidth',14);
set(L,{'color'},mat2cell(colours,ones(1,N),3));
h=legend('Sand','Free space','Compacted fill', 'PVC');
set(h,'color',[0.89,0.94,0.9],'FontWeight','bold','FontSize',14,...
   'FontName','Gautami','Location','NorthEastOutside');
```

2.2.8: geo3D.m

This procedure can be used to display the geometry of the model, generated by GprMax3D. In particular, isosurfaces can be plotted, representing the various parts/objects of the model's geometry. For large models with several details, this procedure doesn't provide a clear representation of the scenario.

```
% ------geo3D------
%
% This Matlab procedure uses data generated by 'GprMax3D',
% electromagnetic wave simulator for Ground Penetrating Radar (GPR) modelling,
% in order to display the geometry of the model.
%
% European Cooperation in Science and Technology (COST)
% COST Action TU1208 "Civil Engineering Applications of Ground Penetrating Radar"
% 2013 - 2017, www.GPRadar.eu, Chair: Lara Pajewski, Italy
```

```
clear all;
% name = 'filename.geo', where filename is the name of file generated by 'GprMax3D'
name = 'filename.geo';
[mesh,ID,header,media] = GprMax3g(name);
% extracts the model's geometry data from the function GprMax3g
C(:,:,:) = mesh(:,:,:);
% creates vectors relative to the size of the model's domain
x=(0:header.nx) * header.dx;
y=(0:header.ny) * header.dy;
z=(0:header.nz) * header.dz;
% gets the size of the vectors
X=max(size(x));
Y=max(size(y));
Z=max(size(z));
figure;
% isosurface(C,isovalue) computes isosurface data from the volume data C
% at the isosurface value specified in isovalue, i.e., isosurface connects points
% that have the specified value much the way contour lines connect points
% of equal elevation. By changing the isovalue it is possible to view just
% some parts/objects of the model's geometry.
p=patch(isosurface(C,2));
set(p,'facecolor','b','edgecolor',[0.68,0.92,1]);
zlabel('z','fontsize',18);
ylabel('x','fontsize',18);
xlabel('y','fontsize',18);
grid on;
axis([0 Y 0 X 0 Z]);
% By definition: "isosurface(V,isovalue) assumes
% the arrays X, Y, and Z are defined as [X,Y,Z] = meshgrid(1:n,1:m,1:p)
% where [m,n,p] = size(V).". Hence, flip/invert X and Y in axis.
```

2.2.9: geo3Dslice.m

This procedure can be used to display three sections (in the *xy*, *xz* and *yz* planes) of the model's geometry, generated by GprMax3D.

```
% ------geo3Dslice------
%
% This Matlab procedure uses data generated by 'GprMax3D',
% electromagnetic wave simulator for Ground Penetrating Radar (GPR) modelling,
% in order to display three slices (xy-,xz- and yz-plane) of the model's geometry.
%
% European Cooperation in Science and Technology (COST)
% COST Action TU1208 "Civil Engineering Applications of Ground Penetrating Radar"
% 2013 - 2017, www.GPRadar.eu, Chair: Lara Pajewski, Italy

clear all;
% name = 'filename.geo', where filename is the name of file generated by 'GprMax3D'
```

16

```
name = 'filename.geo';
[mesh,ID,header,media] = GprMax3g(name);
% you have to specify here the coordinates at which you want to produce
% a slice of the model's geometry
x = 0.3;  % yz-plane at the given x-coordinate [m]
y = 0.2;  % xz-plane at the given y-coordinate [m]
z = 0.42; % xy-plane at the given z-coordinate [m]
% converts coordinates from [m] into the corresponding number of Yee cells
cx=round(x/header.dx);
cy=round(y/header.dy);
cz=round(z/header.dz);
% creates vectors relative to the size of the model's domain
X=(0:header.nx) * header.dx;
Y=(0:header.ny) * header.dy;
Z=(0:header.nz) * header.dz;
% extracts the model's geometry data from the function GprMax3g
meshxz(:,:) = mesh(:,cy,:);
meshyz(:,:) = mesh(cx,:,:);
meshxy(:,:)= mesh(:,:,cz);
% transposes the matrices
planexz= meshxz'; planeyz= meshyz'; planexy= meshxy';
figure; imagesc(X,Z,planexz);
colormap gray
set(gca,'YDir','normal');
colormap (flipud(gray));
axis image;
title(['xz-plane at y=' num2str(y) 'm'], 'fontsize',20)
xlabel('[m]','fontsize',18)
ylabel('[m]','fontsize',18)
figure; imagesc(Y,Z,planeyz);
colormap gray
set(gca,'YDir','normal');
colormap (flipud(gray));
axis image
title(['yz-plane at x=' num2str(x) 'm'], 'fontsize',20)
xlabel('[m]','fontsize',18)
ylabel('[m]','fontsize',18)
figure; imagesc(X,Y,planexy);
set(gca,'YDir','normal');
colormap gray
colormap (flipud(gray));
axis image
title(['xy-plane at z=' num2str(z) 'm'], 'fontsize',20)
xlabel('[m]','fontsize',18)
ylabel('[m]','fontsize',18)
```

2.2.10: snapshot2D.m

This procedure can be used to display a map of the electric field at a given time instant. In order to obtain information about the electromagnetic field within an area of the model at a given time instant, the #snapshot: command has to be introduced in the input GprMax file (as explained in the GprMax user guide).

```
% ------snapshot2D------
%
% This Matlab procedure uses data generated by 'GprMax2D',
% electromagnetic wave simulator for Ground Penetrating Radar (GPR) modelling,
% in order to display a snapshot of the electric field at a given time instant.
%
% European Cooperation in Science and Technology (COST)
% COST Action TU1208 "Civil Engineering Applications of Ground Penetrating Radar"
% 2013 - 2017, www.GPRadar.eu, Chair: Lara Pajewski, Italy

clear all;
% name = 'filename.out', where filename is the name of file generated by 'GprMax2D'
name = 'filename.out';
[Header, Fields] = GprMax( name )
samplex= Header.Snapxsam;    %  sampling intervals in the x direction
sampley= Header.Snapysam;    %  sampling intervals in the y direction
% extracts the values of the field component Ez through the function GprMax
E(:,:) = Fields.ez(:,:);
% creates vectors relative to the size of the chosen snapshot area
for j= 1:samplex
X(j)= Header.Snapx1*Header.dx+ (j-1)*Header.Snapxs*Header.dx;
end
for i= 1:sampley
Y(i)= Header.Snapy1*Header.dy+ (i-1)*Header.Snapys*Header.dy;
end
figure;
imagesc(X,Y,E);
axis xy;
set(gca,'YDir','normal');
title('Snapshot','fontsize',20);
ylabel('[m]','fontsize',18);
xlabel('[m]','fontsize',18);
daspect([1 1 1]);
% sets the data aspect ratio in the current axes to the specified value
% colorbar ('location', 'southoutside');
% grid on;
```

2.2.11: snapshot3D.m

This procedure can be used to display maps of a component of the electromagnetic field at a given time instant, on a *xy*, *xz* and *yz* plane. In order to obtain information about the electromagnetic field within a volume of the model at a given time instant, the #snapshot: command has to be introduced in the input GprMax file (as explained in the GprMax user guide). Such command produces a volume of data for each electromagnetic field component.

```
% ------snapshot3D------
%
% This Matlab procedure uses data generated by 'GprMax3D',
% electromagnetic wave simulator for Ground Penetrating Radar (GPR) modelling,
% in order to display a snapshot of the electric field (on a xy-,xz- and yz-plane)
% at a given time instant.
%
% European Cooperation in Science and Technology (COST)
% COST Action TU1208 "Civil Engineering Applications of Ground Penetrating Radar"
% 2013 - 2017, www.GPRadar.eu, Chair: Lara Pajewski, Italy

clear all;
% name = 'filename.out', where filename is the name of file generated by 'GprMax3D'
name = 'filename.out';
[Header, Fields] = GprMax( name )
% specify here the coordinates at which you want to produce a snapshot
x = 0.6; % yz-plane at the given x-coordinate [m]
y = 0.6; % xz-plane at the given y-coordinate [m]
z = 0.6; % xy-plane at the given z-coordinate [m]
% converts coordinates from [m] into the corresponding number of Yee cells
cx=round(x/Header.dx);
cy=round(y/Header.dy);
cz=round(z/Header.dz);
samplex= Header.Snapxsam;%sampling intervals in the x direction
sampley= Header.Snapysam;%sampling intervals in the y direction
samplez= Header.Snapzsam;%sampling intervals in the z direction
%extracts the values of the field components from the function GprMax
planexy(:,:) = Fields.ex(:,:,cz);
planexz(:,:) = Fields.ex(:,cy,:);
planeyz(:,:) = Fields.ex(cx,:,:);
% transposes the matrices
planexy = planexy';
planexz = planexz';
planeyz = planeyz';
% creates vectors relative to the size of the chosen snapshot area
```

19

```
for j= 1:samplex
X(j)= Header.Snapx1*Header.dx+ (j-1)*Header.Snapxs*Header.dx;
end
for i= 1:sampley
Y(i)= Header.Snapy1*Header.dy+ (i-1)*Header.Snapys*Header.dy;
end
for k= 1:samplez
Z(k)= Header.Snapz1*Header.dz+ (k-1)*Header.Snapzs*Header.dz;
end
figure;
imagesc(X,Y,planexy); axis xy; set(gca,'YDir','normal');
title('Snapshot (xy-plane)','fontsize',20);
ylabel('[m]','fontsize',18); xlabel('[m]','fontsize',18);
daspect([1 1 1]);
%colorbar ('location', 'southoutside');
%grid on;
figure; imagesc(X,Z,planexz);  axis xy; set(gca,'YDir','normal');
title('Snapshot (xz-plane)','fontsize',20); ylabel('[m]','fontsize',18); xlabel('[m]','fontsize',18);
daspect([1 1 1]);
figure; imagesc(Y,Z,planeyz); axis xy; set(gca,'YDir','normal');
title('Snapshot (yz-plane)','fontsize',20); ylabel('[m]','fontsize',18); xlabel('[m]','fontsize',18);
daspect([1 1 1]);
```

2.2.12: `video2D.m`

This procedure can be used to create a movie of the electric field, showing how the map of the electric field in a certain region of the model changes with time. In order to obtain information about the electromagnetic field within an area of the model in N different time instants, the #snapshot: command has to be introduced N times in the input GprMax file.

```
% ------video2D------
%
% This Matlab procedure uses data generated by 'GprMax2D',
% electromagnetic wave simulator for Ground Penetrating Radar (GPR) modelling,
% in order to create a video of the electromagnetic field.
%
% European Cooperation in Science and Technology (COST)
% COST Action TU1208 "Civil Engineering Applications of Ground Penetrating Radar"
% 2013 - 2017, www.GPRadar.eu

clear all;
% assign a name to your video - 'videoname.avi'
vidObj = VideoWriter('videoname.avi');
vidObj.FrameRate=5;  % rate of playback for the video in frames per second
open(vidObj); snapshotdirectory = 'C:\Users\Lara\GprMax matlab\snapshot';
snapshotfiles = fullfile(snapshotdirectory, '*.out'); files = dir(snapshotfiles);
for k=1:length(files)
```

```
name=(['snap' num2str(k) '.out']);
   [Header, Fields] = GprMax(name);
   samplex= Header.Snapxsam; % sampling intervals in the x direction
   sampley= Header.Snapysam; % sampling intervals in the y direction
   E(:,:) = Fields.ez(:,:);
% creates vectors relative to the size of the chosen snapshot area
for j= 1:samplex
X(j)= Header.Snapx1*Header.dx+ (j-1)*Header.Snapxs*Header.dx;
end
for i= 1:sampley
Y(i)= Header.Snapy1*Header.dy+ (i-1)*Header.Snapys*Header.dy;
end
imagesc(X,Y,E); axis xy; set(gca,'YDir','normal'); colormap jet;
daspect([1 1 1]); % sets the data aspect ratio in the current axes to the specified value
F(k) = getframe;
end
writeVideo(vidObj,F); close(vidObj);
```

2.3: DEFINITION OF TEST SCENARIOS FOR THE COMPARISON OF DIFFERENT ELECTROMAGNETIC FORWARD- AND INVERSE-SCATTERING METHODS

The third part of the STSM was devoted to the definition of a set of test scenarios. Working Group Members who are developing electromagnetic forward/inverse scattering techniques and imaging methods will be provided with the geometrical and physical characteristics defining these scenarios, as well as with results calculated by using the GprMax software; the accuracy and applicability of different techniques will be tested and compared on the proposed scenarios. The aim of this initiative is not that of identifying the best methods, but more properly to indicate the range of reliability of each approach, highlighting its advantages and drawbacks. The realisation of the proposed structures and the acquisition of GPR experimental data will allow a further effective benchmark for forward/inverse scattering methods and imaging techniques.

The set of test scenarios is constituted by a number of concrete structures, hereinafter called cells. Structural investigation of reinforced concrete through GPR is well-established and increasingly used [6], the principal current applications are summarized in Table I.

Table I : Some applications of GPR for structural concrete

Greatest reliability	←	→	Least reliability
Estimation of element thickness from one surface			
Location of reinforcing bars and metallic ducts; estimation of depth			
Determination of major construction features			
Location of moisture variations			**Increasingly experimental**
Location of voids			
Estimation of major voids size			
Location of honeycombing/cracking/chlorides			
Estimation of bar size			
Estimation of chloride concentrations			
Location of reinforcement corrosion			

The size of each cell is 60 x 100 x 18 cm and the content varies with growing complexity, from a simple cell with few rebars of different diameters embedded in concrete at increasing depths, to a final cell with a quite complicated pattern, including a layer of tendons between two overlying meshes of rebars. Other cells, of intermediate complexity, contain pvc ducts (air filled or hosting rebars), steel objects commonly used in civil engineering (as a pipe, an angle bar, a box section and an u-channel), as well as void and honeycombing defects. One of the cells has a steel mesh embedded in it, overlying two rebars placed diagonally across the comers of the structure. Two cells include a couple of rebars bent into a right angle and placed on top of each other, with a square/round circle lying at the base of the concrete slab. Inspiration for some of these cells is taken from the very interesting experimental work presented in [7].

For each cell, a subset of models is defined, starting from a simple representation of the cell and ending with a more realistic one. In particular, the model's complexity increases from the geometrical point of view, as well as in terms of how the constitutive parameters of the involved media and the GPR antennas are described.

Some cells can be simulated in both two and three dimensions. The concrete slab can be approximated as a finite-thickness layer having infinite extension on the transverse plane, thus neglecting how edges affect radargrams, or else its finite size can be fully taken into account.

The permittivity of concrete can be defined through a constant real value, or else its frequency-dispersion properties can be taken into account by incorporating into the model Debye approximations [8] or by adopting the Joenscher model [9, 10].

The electromagnetic source can be represented as a simple line of current (in the case of two-dimensional models), a Hertzian dipole, a bow tie antenna, or else, the realistic description of a commercial antenna can be included in the model [11].

The simplest three cells are sketched in Figure 1. They can be simulated both in two and three dimensions. Cell 1.1 includes three identical pipes buried at increasing depths, as well as smaller and larger bars. Cell 1.2 consists of four linear targets as follows: a rebar, two PVC ducts (one air filled and the other with a steel rod inserted), a steel water pipe. Cell 1.3 hosts typical reinforced concrete elements as an angle bar, a box section and a u-channel. For these cells, input GprMax2D and GprMax3D files are reported in Section 2.4 of this document, along with some numerical results obtained with GprMax2D, for the simplest case of concrete permittivity defined through a constant real value. Further results obtained by adopting a Debye model for the permittivity of concrete are also available but they are not included here, for brevity reasons. Results obtained by executing the 3D models are available, too.

2.4: MODELLING THE DEFINED TEST SCENARIOS WITH GPRMAX

2.4.1: Cell 1.1

For Cell 1.1, both 2D and a 3D models have been created. The concrete slab has been approximated as a finite-thickness layer having infinite extension on the transverse plane, thus neglecting how edges affect radargrams, or else its finite size has

been fully taken into account. The compacted fill has always been modelled as having infinite extension.
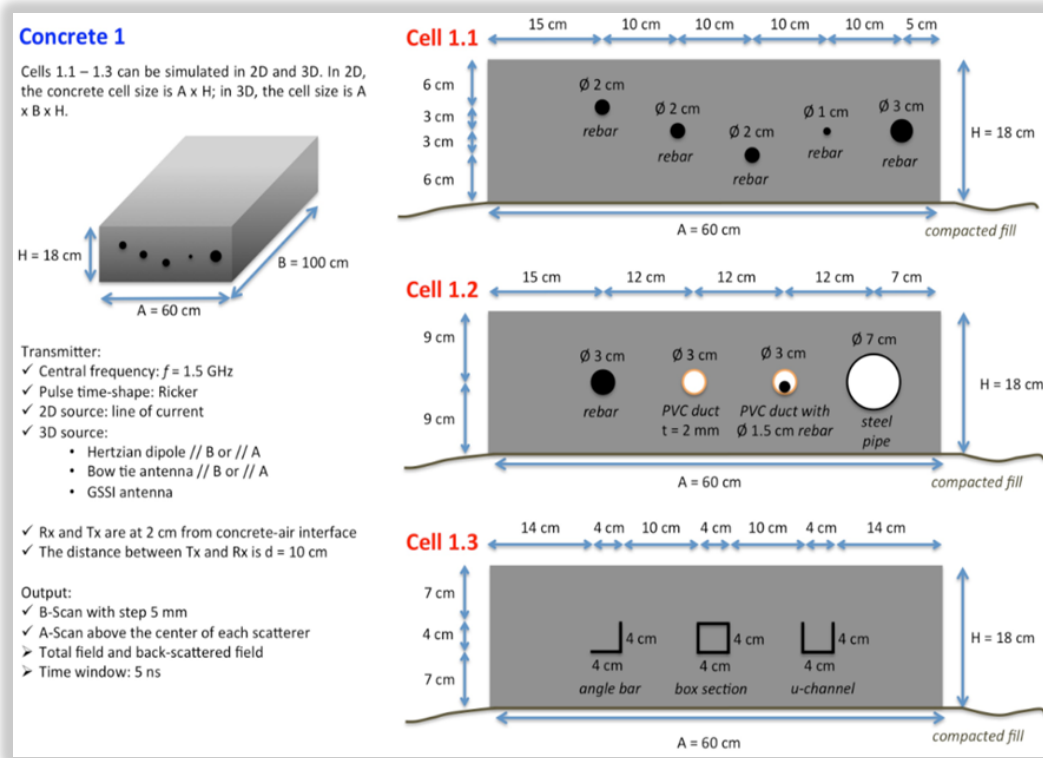
Figure 1 – Sketch of Cells 1.1 – 1.3.

All the numerical results have been obtained for a frequency f = 1.5 GHz and a Ricker shape of the time pulse emitted by the transmitter.

The transmitting and receiving antennas are at 2 cm from concrete-air interface, the distance between them is 10 cm.

B-scans with 5 cm step have been calculated, in the transverse plane, as well as A-scans above the center of each scatterer, for both the total and the back-scattered electric field, on a 5 ns time window.

The relative permittivity of concrete is assumed to be ε_r=6 and its conductivity is σ=0.01 S/m; the relative permittivity of the compacted fill is ε_r=16 and its conductivity is σ=0.005 S/m. Metallic objects are assumed to be perfectly conducting.

For the finite-size model, GprMax2D and GprMax3D input files are reported in Table II. The spatial discretisation (size of Yee cells) is 0.0005 m along *x, y* and *z*, representing a good compromise between accuracy and execution time. The time discretisation is fixed by applying the stability CFL (Courant, Freidrichs and Lewy) condition. The simulation space is surrounded with a layer of non physical absorbing material occupying 10 Yee cells (i.e., Perfectly Matched Layer, PML, Absorbing Boundary Conditions, ABCs, are employed).

For this model, Figure 2 shows the B-scan of the total electric field and Figure 3 shows the B-scan of the electric field back-scattered by the embedded bars, obtained with GprMax2D. Figure 4 shows the 2D output geometry.

For the infinite model of Cell 1.1, GprMax2D and GprMax3D input files are reported in Table III. The spatial and time discretisation are the same and a PML occupying 10 Yee cells is again used.

For this model, Figure 5 shows the B-scan of the total electric field and Figure 6 shows the B-scan of the electric field back-scattered by the embedded bars, obtained with GprMax2D, to be compared with those shown in Figures 2 and 3, respectively. Figure 7 shows the 2D output geometry.
The A-scans calculated above the axes of all the rods embedded in the concrete slab, are reported in Figures 8-15. In particular, Figure 8 compares A-scans of the total electric field above rebars having the same diameter (Ø 2 cm) and buried at different depths (calculated by taking into account the finite size of concrete slab). Figure 9 shows the same as in Figure 8, for the back-scattered electric field. In Figure 10, results obtained for the finite-size concrete slab are compared with those obtained for the infinite slab. Figures 12-15 present A-scans over the three rebars having different size (Ø 1, 2 and 3 cm) and buried at the same depth (d=9 cm).

25

Table II

Input GprMax2D and GprMax3D files for Cell 1.1,
taking into account the finite size of the concrete slab.

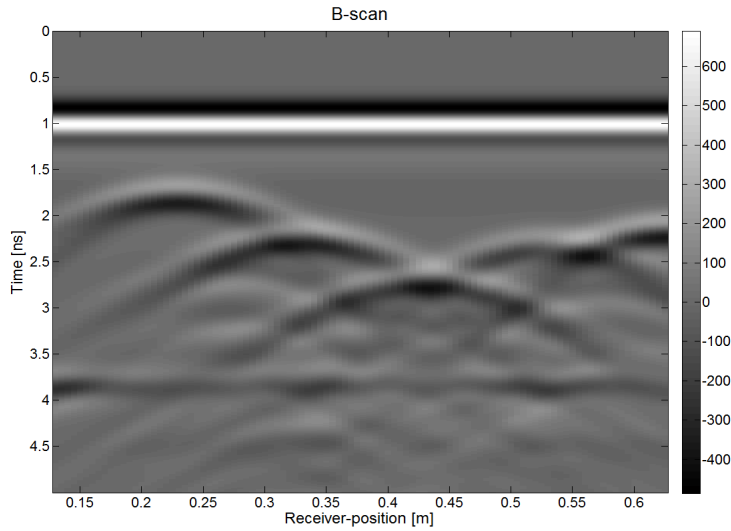| GprMax 2D - Cell 1.1 (finite size)	GprMax 3D - Cell 1.1 (finite size)
#medium: 6.0 0.0 0.0 0.01 1.0 0.0 concrete #medium: 16.0 0.0 0.0 0.005 1.0 0.0 compacted_fill --- #domain: 0.66 0.28 #dx_dy: 0.0005 0.0005 #time_window: 5e-9 #abc_type: pml #pml_layers: 10 --- #box: 0.0 0.0 0.66 0.05 compacted_fill #box: 0.03 0.05 0.63 0.23 concrete --- #cylinder: 0.18 0.17 0.01 pec #cylinder: 0.28 0.14 0.01 pec #cylinder: 0.38 0.11 0.01 pec #cylinder: 0.48 0.14 0.005 pec #cylinder: 0.58 0.14 0.015 pec --- #line_source: 1.0 1500e6 ricker MyLineSource --- #analysis: 100 cell1.1_2D.out b #tx: 0.03 0.25 MyLineSource 0.0 5e-9 #rx: 0.13 0.25 #tx_steps: 0.005 0.0 #rx_steps: 0.005 0.0 #end_analysis: --- #geometry_file: cell1.1_2D.geo #title: Cell 1.1_2D #messages: y	#medium: 6.0 0.0 0.0 0.01 1.0 0.0 concrete #medium: 16.0 0.0 0.0 0.005 1.0 0.0 compacted_fill --- #domain: 1.06 0.66 0.28 #dx_dy_dz: 0.0005 0.0005 0.0005 #time_window: 5e-9 #abc_type: pml #pml_layers: 10 --- #box: 0.0 0.0 0.0 1.06 0.66 0.05 compacted_fill #box: 0.03 0.03 0.05 1.03 0.63 0.23 concrete --- #cylinder: x 0.03 1.03 0.18 0.17 0.01 pec #cylinder: x 0.03 1.03 0.28 0.14 0.01 pec #cylinder: x 0.03 1.03 0.38 0.11 0.01 pec #cylinder: x 0.03 1.03 0.48 0.14 0.005 pec #cylinder: x 0.03 1.03 0.58 0.14 0.015 pec --- #hertzian_dipole: 1.0 1500e6 ricker MyDipole --- #analysis: 100 cell1.1_3D.out b #tx: x 0.5 0.03 0.25 MyDipole 0.0 5e-9 #rx: 0.5 0.13 0.25 #tx_steps: 0.0 0.005 0.0 #rx_steps: 0.0 0.005 0.0 #end_analysis: --- #geometry_file: cell1.1_3D.geo #title: Cell 1.1_3D #messages: y

26

Figure 2 – B-scan of the total electric field obtained with
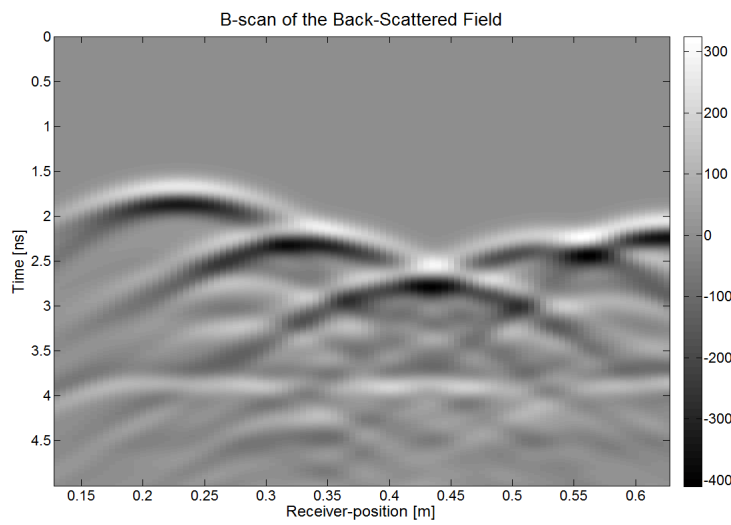GprMax2D for Cell 1.1 (finite-size concrete slab).
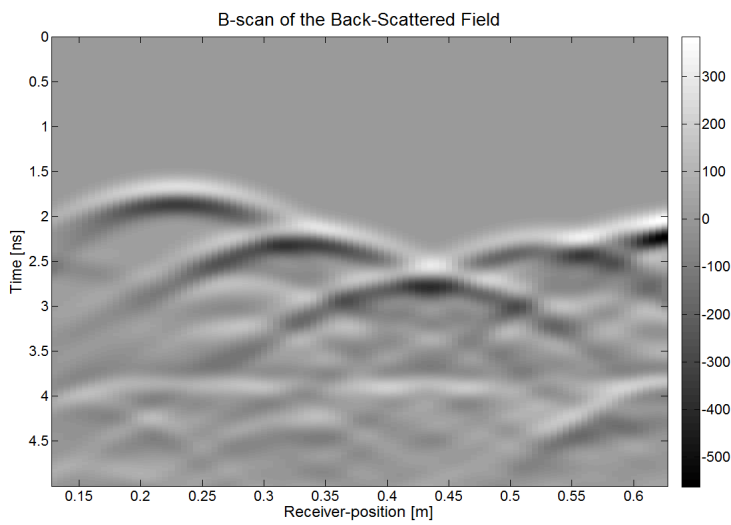
Figure 3 – B-scan of the back-scattered field obtained with
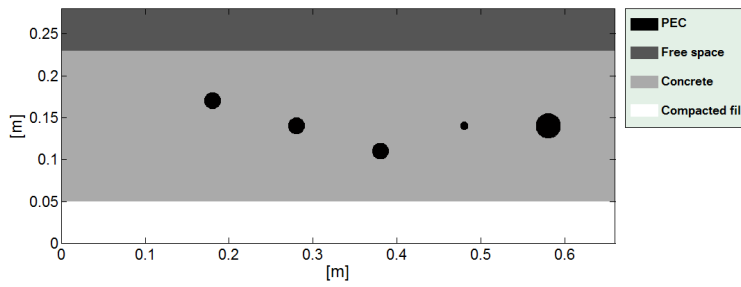GprMax2D for Cell 1.1 (finite-size concrete slab).

27
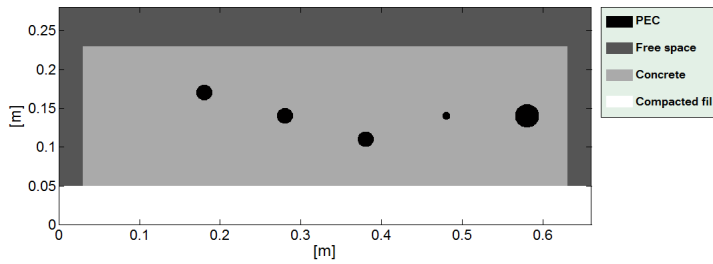
Figure 4 – Output geometry of Cell 1.1 (finite-size concrete slab).

Table III - Input GprMax2D and GprMax3D files for Cell 1.1,
assuming an infinite extension of the concrete slab.

GprMax 2D - Cell 1.1 (infinite cell)	GprMax 3D - Cell 1.1 (infinite cell)
#medium: 6.0 0.0 0.0 0.01 1.0 0.0 concrete #medium: 16.0 0.0 0.0 0.005 1.0 0.0 c_fill #domain: 0.66 0.28 #dx_dy: 0.0005 0.0005 #time_window: 5e-9 #abc_type: pml #pml_layers: 10 --- #box: 0.0 0.0 0.66 0.05 c_fill #box: 0.0 0.05 0.66 0.23 concrete #cylinder: 0.18 0.17 0.01 pec #cylinder: 0.28 0.14 0.01 pec #cylinder: 0.38 0.11 0.01 pec #cylinder: 0.48 0.14 0.005 pec #cylinder: 0.58 0.14 0.015 pec --- #line_source: 1.0 1500e6 ricker LineSource #analysis: 100 cell1.1_2D_concrete.out b #tx: 0.03 0.25 LineSource 0.0 5e-9 #rx: 0.13 0.25 #tx_steps: 0.005 0.0 #rx_steps: 0.005 0.0 #end_analysis: --- #geometry_file: cell1.1_2D_concrete.geo #title: Cell 1.1_2D #messages: y	#medium: 6.0 0.0 0.0 0.01 1.0 0.0 concrete #medium: 16.0 0.0 0.0 0.005 1.0 0.0 c_fill #domain: 1.06 0.66 0.28 #dx_dy_dz: 0.0005 0.0005 0.0005 #time_window: 5e-9 #abc_type: pml #pml_layers: 10 --- #box: 0.0 0.0 0.0 1.06 0.66 0.05 c_fill #box: 0.0 0.0 0.05 1.06 0.66 0.23 concrete #cylinder: x 0.0 1.06 0.18 0.17 0.01 pec #cylinder: x 0.0 1.06 0.28 0.14 0.01 pec #cylinder: x 0.0 1.06 0.38 0.11 0.01 pec #cylinder: x 0.0 1.06 0.48 0.14 0.005 pec #cylinder: x 0.0 1.06 0.58 0.14 0.015 pec --- #hertzian_dipole: 1.0 1500e6 ricker Dipole #analysis: 100 cell1.1_3D_concrete.out b #tx: x 0.5 0.03 0.25 Dipole 0.0 5e-9 #rx: 0.5 0.13 0.25 #tx_steps: 0.0 0.005 0.0 #rx_steps: 0.0 0.005 0.0 #end_analysis: --- #geometry_file: cell1.1_3D_concrete.geo #title: Cell 1.1_3D #messages: y

Figure 5 – B-scan of the total electric field obtained with
GprMax2D for Cell 1.1 (infinite concrete slab).

Figure 6 – B-scan of the back-scattered field obtained with
GprMax2D for Cell 1.1 (infinite concrete slab).
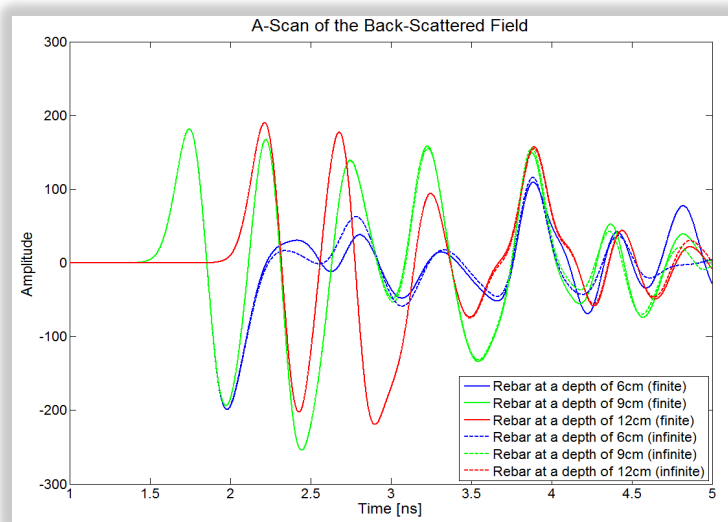
29

Figure 7 – Output gometry of Cell 1.1 (infinite concrete slab).
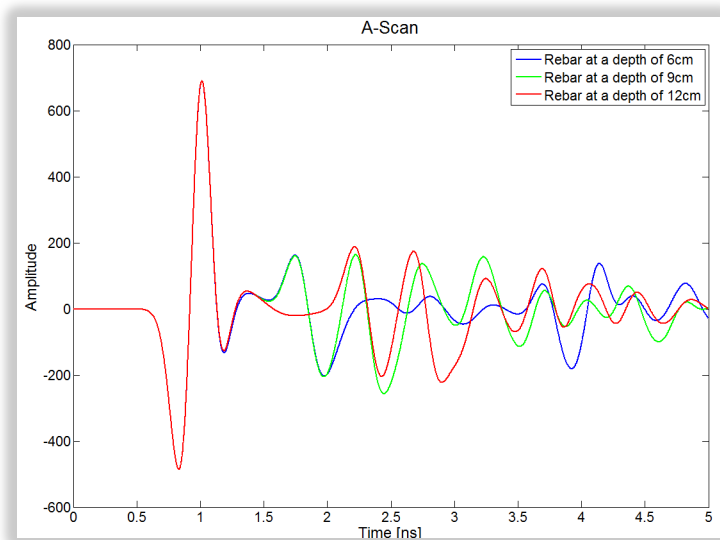
Figure 8 – A-scan of the total electric field, calculated above bars having the same diameter (Ø 2cm) and buried at different depths (finite-size concrete slab).
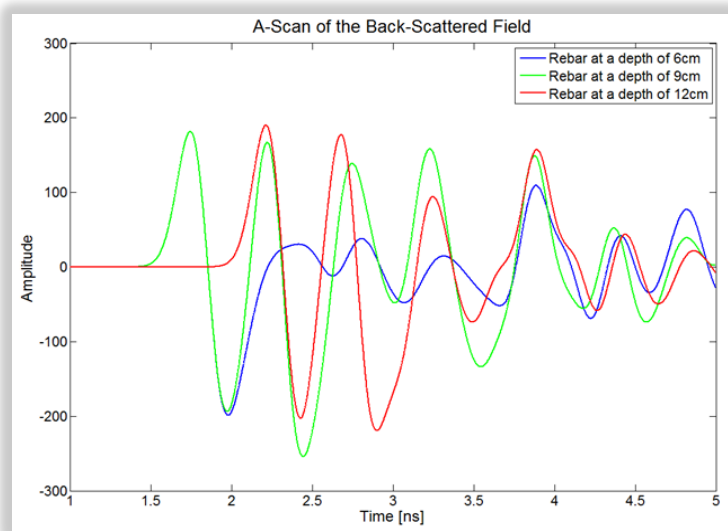
Figure 9 – Same as in Figure 8, for the backscattered field.

Figure 10 – A-scans of the total electric field, calculated above bars having the same diameter (Ø 2cm) and buried at different depths: comparison between finite and infinite models.
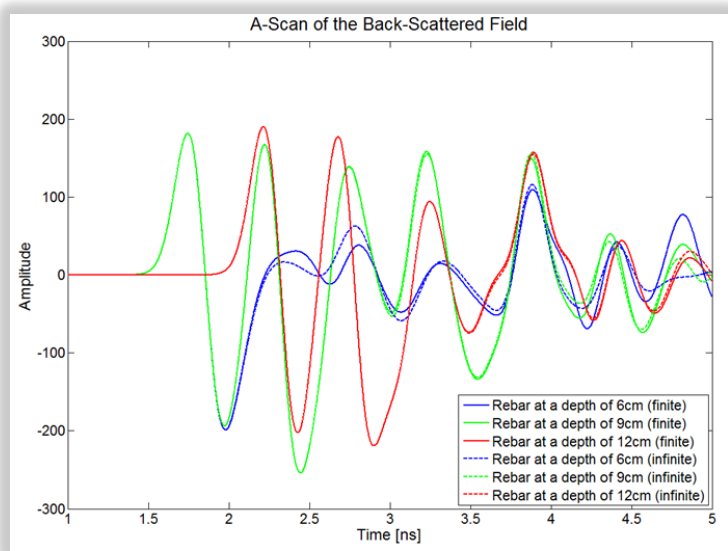
Figure 11 – Same as in Figure 10, for the backscattered field.
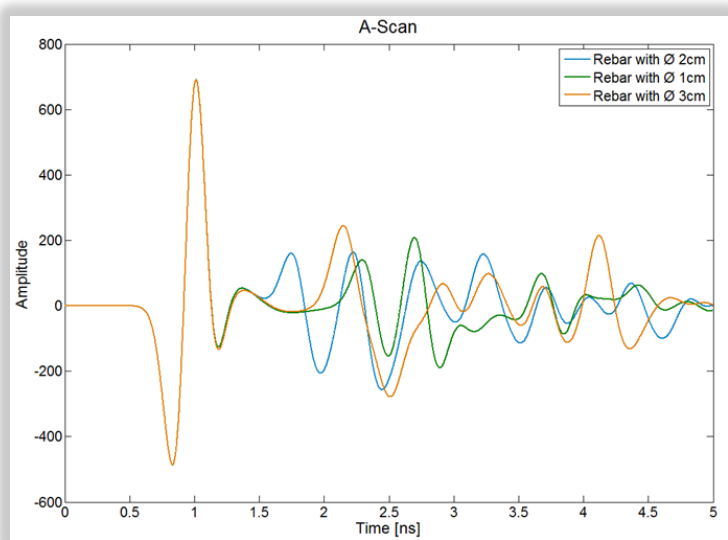
Figure 12 – A-scans above bars with different size and same
burial depth (total electric field; finite-size concrete slab).

32
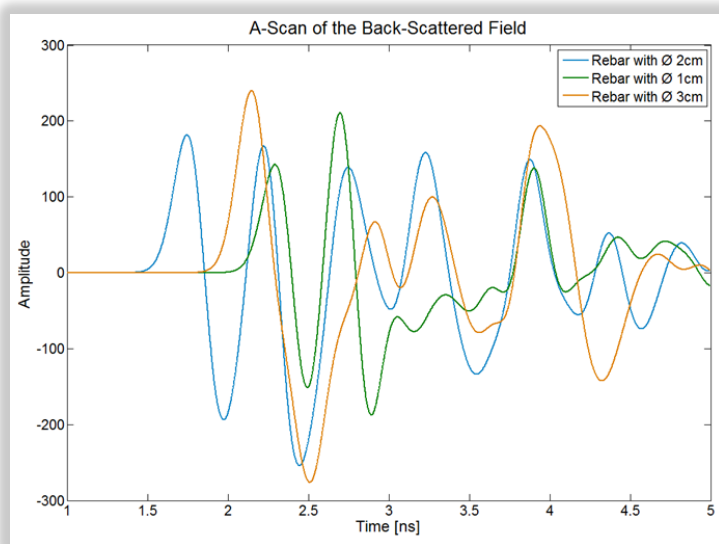
Figure 13 – Same as in Figure 12, for the backscattered field.
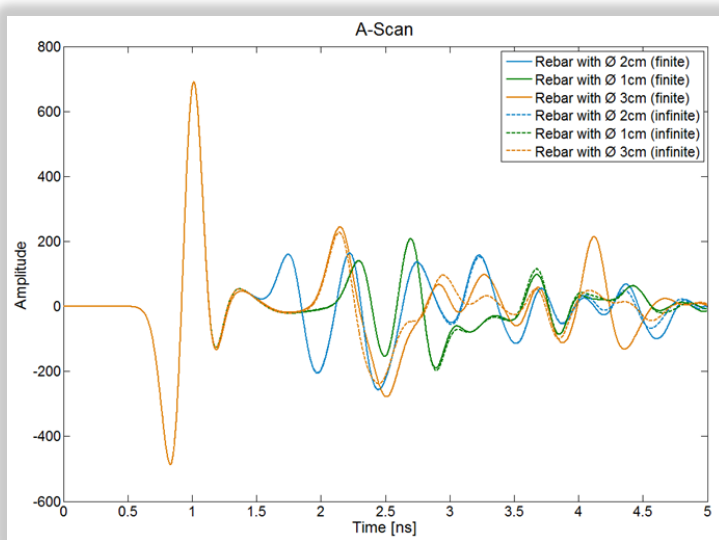
Figure 14 – A-scans on bars with different size and same depth:
comparison between finite and infinite slab (total electric field).
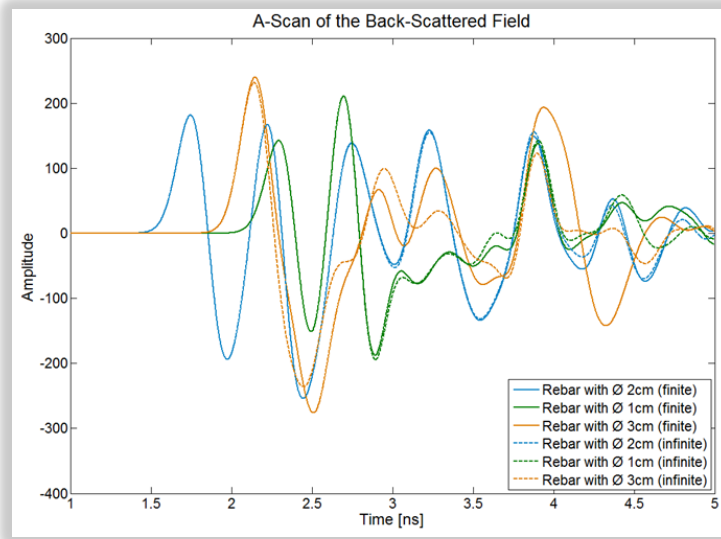
Figure 15 – Same as in 14, for the backscattered field.

2.4.2: Cell 1.2

For Cell 1.2, an analogous analysis has been carried out. Both 2D and 3D models have been created. The concrete slab has been approximated as a finite-thickness layer having infinite extension on the transverse plane, or else its finite size has been taken into account. The relative permittivity of PVC was assumed to be $\varepsilon_r=3$.

For the finite-size model, GprMax input files are reported In Table IV. Results are shown in Figure 16, where the B-scan of the total electric field is reported, and in Figure 17, where the B-scan of the electric field back-scattered by the embedded targets is shown, obtained with GprMax2D. Figure 18 is the 2D output geometry.

For the model with infinite concrete slab, GprMax input files are reported In Table V. Results are shown in Figure 19, where the B-scan of the total electric field is reported, and in Figure 20, where the B-scan of the electric field back-scattered by the embedded targets is shown, obtained with GprMax2D.

Table IV
Input GprMax2D and GprMax3D files for Cell 1.2, taking into
account the finite size of the concrete slab.

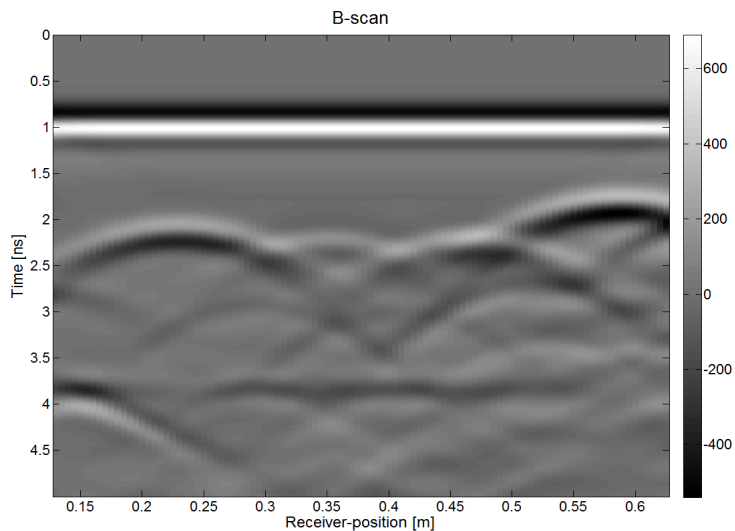| GprMax 2D - Cell 1.2 (finite)	GprMax 3D - Cell 1.2 (infinite)
#medium: 6.0 0.0 0.0 0.01 1.0 0.0 concrete #medium: 16.0 0.0 0.0 0.005 1.0 0.0 c_fill #medium: 3.0 0.0 0.0 0.0 1.0 0.0 pvc --- #domain: 0.66 0.28 #dx_dy: 0.0005 0.0005 #time_window: 5e-9 #abc_type: pml #pml_layers: 10 --- #box: 0.0 0.0 0.66 0.05 c_fill #box: 0.03 0.05 0.63 0.23 concrete --- #cylinder: 0.18 0.14 0.015 pec #cylinder: 0.3 0.14 0.015 pvc #cylinder: 0.3 0.14 0.013 free_space #cylinder: 0.42 0.14 0.015 pvc #cylinder: 0.42 0.14 0.013 free_space #cylinder: 0.42 0.1345 0.0075 pec #cylinder: 0.54 0.14 0.035 pec #cylinder: 0.54 0.14 0.033 free_space --- #line_source: 1.0 1500e6 ricker LineSource --- #analysis: 100 cell1.2_2D.out b #tx: 0.03 0.25 LineSource 0.0 5e-9 #rx: 0.13 0.25 #tx_steps: 0.005 0.0 #rx_steps: 0.005 0.0 #end_analysis: --- #geometry_file: cell1.2_2D.geo #title: Cell 1.1_2D #messages: y	#medium: 6.0 0.0 0.0 0.01 1.0 0.0 concrete #medium: 16.0 0.0 0.0 0.005 1.0 0.0 c_fill #medium: 3.0 0.0 0.0 0.0 1.0 0.0 pvc --- #domain: 1.06 0.66 0.28 #dx_dy_dz: 0.0005 0.0005 0.0005 #time_window: 5e-9 #abc_type: pml #pml_layers: 10 --- #box: 0.0 0.0 0.0 1.06 0.66 0.05 c_fill #box: 0.03 0.03 0.05 1.03 0.63 0.23 concrete --- #cylinder: x 0.03 1.03 0.18 0.14 0.015 pec #cylinder: x 0.03 1.03 0.3 0.14 0.015 pvc #cylinder: x 0.03 1.03 0.3 0.14 0.013 free_space #cylinder: x 0.03 1.03 0.42 0.14 0.015 pvc #cylinder: x 0.03 1.03 0.42 0.14 0.013 free_space #cylinder: x 0.03 1.03 0.42 0.1345 0.0075 pec #cylinder: x 0.03 1.03 0.54 0.14 0.035 pec #cylinder: x 0.03 1.03 0.54 0.14 0.033 free_space --- #hertzian_dipole: 1.0 1500e6 ricker Dipole --- #analysis: 100 cell1.2_3D.out b #tx: x 0.5 0.03 0.25 Dipole 0.0 5e-9 #rx: 0.5 0.13 0.25 #tx_steps: 0.0 0.005 0.0 #rx_steps: 0.0 0.005 0.0 #end_analysis: --- #geometry_file: cell1.2_3D.geo #title: Cell 1.2_3D #messages: y

Figure 16 – B-scan of the total electric field obtained with GprMax2D for Cell 1.2 (finite-size concrete slab).
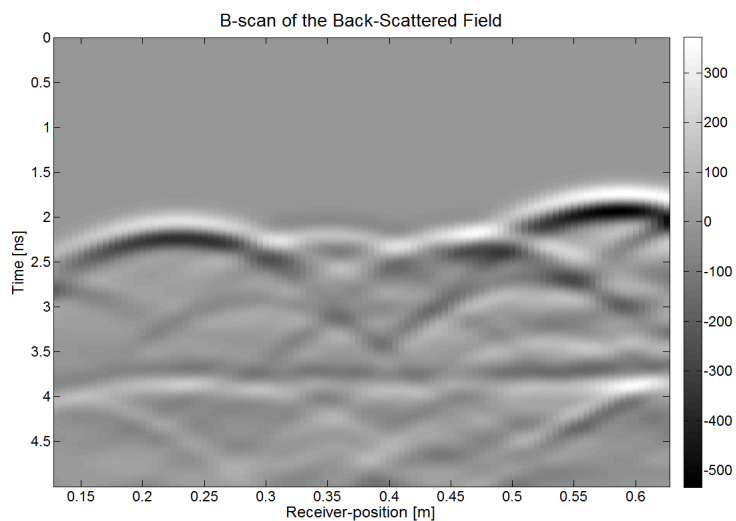

Figure 17 – B-scan of the back-scattered electric field obtained with GprMax2D for Cell 1.2 (finite-size concrete slab).
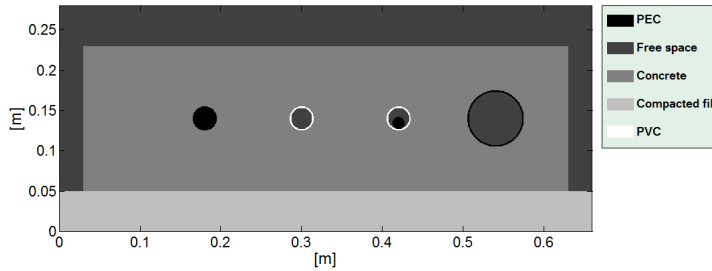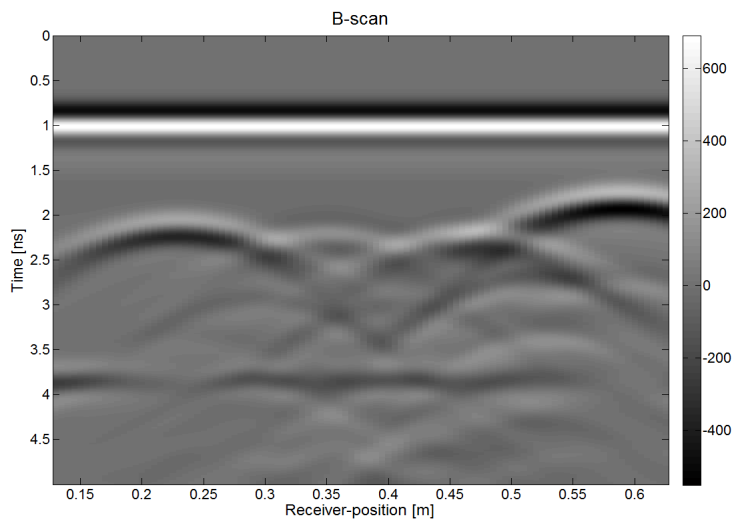
36

Figure 18 – Output geometry of Cell 1.2 (finite-size concrete slab).

Table V - Input GprMax2D and GprMax3D files for Cell 1.2, assuming an infinite extension of the concrete slab.

GprMax 2D	GprMax 3D
#medium: 6.0 0.0 0.0 0.01 1.0 0.0 concrete #medium: 16.0 0.0 0.0 0.005 1.0 0.0 c_fill #medium: 3.0 0.0 0.0 0.0 1.0 0.0 pvc -- #domain: 0.66 0.28 #dx_dy: 0.0005 0.0005 #time_window: 5e-9 #abc_type: pml #pml_layers: 10 -- #box: 0.0 0.0 0.66 0.05 c_fill #box: 0.0 0.05 0.66 0.23 concrete #cylinder: 0.18 0.14 0.015 pec #cylinder: 0.3 0.14 0.015 pvc #cylinder: 0.3 0.14 0.013 free_space #cylinder: 0.42 0.14 0.015 pvc #cylinder: 0.42 0.14 0.013 free_space #cylinder: 0.42 0.1345 0.0075 pec #cylinder: 0.54 0.14 0.035 pec #cylinder: 0.54 0.14 0.033 free_space -- #line_source: 1.0 1500e6 ricker LineSource #analysis: 100 cell1.2_2D_concrete.out b #tx: 0.03 0.25 LineSource 0.0 5e-9 #rx: 0.13 0.25 #tx_steps: 0.005 0.0 #rx_steps: 0.005 0.0 #end_analysis: #geometry_file: cell1.2_2D_concrete.geo #title: Cell 1.1_2D #messages: y	#medium: 6.0 0.0 0.0 0.01 1.0 0.0 concrete #medium: 16.0 0.0 0.0 0.005 1.0 0.0 c_fill #medium: 3.0 0.0 0.0 0.0 1.0 0.0 pvc -- #domain: 1.06 0.66 0.28 #dx_dy_dz: 0.0005 0.0005 0.0005 #time_window: 5e-9 #abc_type: pml #pml_layers: 10 -- #box: 0.0 0.0 0.0 1.06 0.66 0.05 c_fill #box: 0.0 0.0 0.05 1.06 0.66 0.23 concrete #cylinder: x 0.03 1.03 0.18 0.14 0.015 pec #cylinder: x 0.03 1.03 0.3 0.14 0.015 pvc #cylinder: x 0.03 1.03 0.3 0.14 0.013 free_space #cylinder: x 0.03 1.03 0.42 0.14 0.015 pvc #cylinder: x 0.03 1.03 0.42 0.14 0.013 free_space #cylinder: x 0.03 1.03 0.42 0.1345 0.0075 pec #cylinder: x 0.03 1.03 0.54 0.14 0.035 pec #cylinder: x 0.03 1.03 0.54 0.14 0.033 free_space -- #hertzian_dipole: 1.0 1500e6 ricker Dipole #analysis: 100 cell1.2_3D_concrete.out b #tx: x 0.5 0.03 0.25 Dipole 0.0 5e-9 #rx: 0.5 0.13 0.25 #tx_steps: 0.0 0.005 0.0 #rx_steps: 0.0 0.005 0.0 #end_analysis: #geometry_file: cell1.2_3D_concrete.geo #title: Cell 1.2_3D #messages: y
GprMax 2D - Cell 1.2 (infinite slab)	*GprMax 3D - Cell 1.2 (infinite slab)*

Figure 19 – B-scan of the total electric field obtained with
GprMax2D for Cell 1.2 (infinite concrete slab).
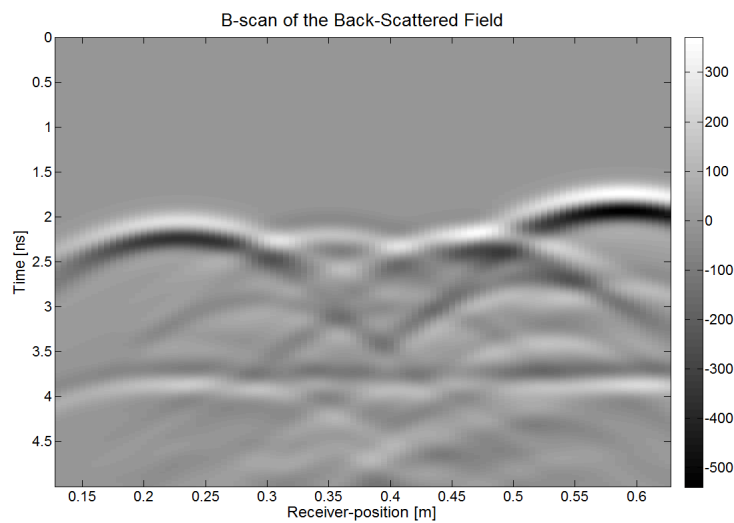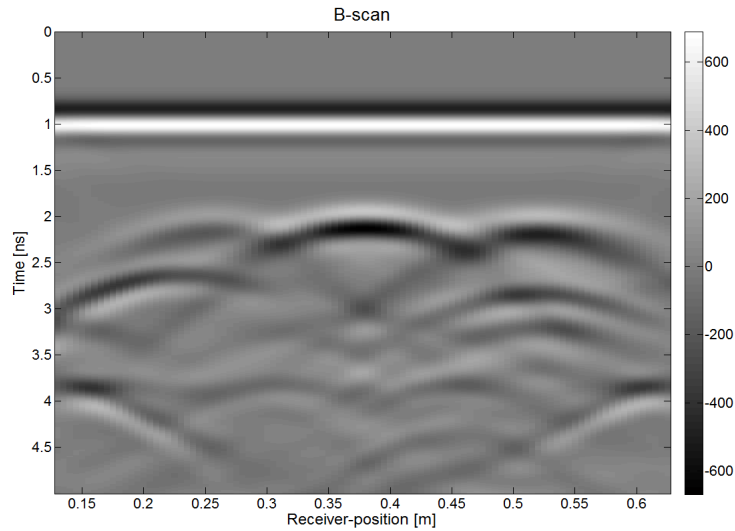

Figure 20 – B-scan of the back-scattered electric field obtained
with GprMax2D for Cell 1.2 (infinite concrete slab).

38

2.4.3: Cell 1.3

For Cell 1.3, the same analysis has been carried out.
For the finite-size model, GprMax input files are reported In Table VI. Results obtained with GprMax2D are shown in Figures 21 and 22, where B-scans of the total and backscattered electric field are reported, respectively; Figure 23 shows the 2D output geometry. Results for the model assuming an infinite extension of the concrete slab are shown in Figures 24 and 25, where B-scans of the total and backscattered electric field are reported, respectively.

Table VI – Input GprMax2D and GprMax3D files for Cell 1.3, taking into account the finite size of the concrete slab.

GprMax 2D - Cell 1.3 (finite)	GprMax 3D - Cell 1.3 (finite)
#medium: 6.0 0.0 0.0 0.01 1.0 0.0 concrete #medium: 16.0 0.0 0.0 0.005 1.0 0.0 c_fill #domain: 0.66 0.28 #dx_dy: 0.0005 0.0005 #time_window: 5e-9 #abc_type: pml #pml_layers: 10 --- #box: 0.0 0.0 0.66 0.05 c_fill #box: 0.03 0.05 0.63 0.23 concrete #box: 0.17 0.12 0.21 0.125 pec #box: 0.205 0.12 0.21 0.16 pec #box: 0.31 0.12 0.35 0.125 pec #box: 0.345 0.12 0.35 0.16 pec #box: 0.31 0.12 0.315 0.16 pec #box: 0.31 0.155 0.35 0.16 pec #box: 0.45 0.12 0.49 0.125 pec #box: 0.485 0.12 0.49 0.16 pec #box: 0.45 0.12 0.455 0.16 pec --- #line_source: 1.0 1500e6 ricker MyLineSource #analysis: 100 cell1.3_2D.out b #tx: 0.03 0.25 MyLineSource 0.0 5e-9 #rx: 0.13 0.25 #tx_steps: 0.005 0.0 #rx_steps: 0.005 0.0 #end_analysis: #geometry_file: cell1.3_2D.geo #title: Cell 1.1_2D #messages: y	#medium: 6.0 0.0 0.0 0.01 1.0 0.0 concrete #medium: 16.0 0.0 0.0 0.005 1.0 0.0 c_fill #domain: 1.06 0.66 0.28 #dx_dy_dz: 0.0005 0.0005 0.0005 #time_window: 5e-9 #abc_type: pml #pml_layers: 10 --- #box: 0.0 0.0 0.0 1.06 0.66 0.05 c_fill #box: 0.03 0.03 0.05 1.03 0.63 0.23 concrete #box: 0.03 0.17 0.12 1.03 0.21 0.125 pec #box: 0.03 0.205 0.12 1.03 0.21 0.16 pec #box: 0.03 0.31 0.12 1.03 0.35 0.125 pec #box: 0.03 0.345 0.12 1.03 0.35 0.16 pec #box: 0.03 0.31 0.12 1.03 0.315 0.16 pec #box: 0.03 0.31 0.155 1.03 0.35 0.16 pec #box: 0.03 0.45 0.12 1.03 0.49 0.125 pec #box: 0.03 0.485 0.12 1.03 0.49 0.16 pec #box: 0.03 0.45 0.12 1.03 0.455 0.16 pec --- #hertzian_dipole: 1.0 1500e6 ricker MyDipole #analysis: 100 cell1.3_3D.out b #tx: x 0.5 0.03 0.25 MyDipole 0.0 5e-9 #rx: 0.5 0.13 0.25 #tx_steps: 0.0 0.005 0.0 #rx_steps: 0.0 0.005 0.0 #end_analysis: #geometry_file: cell1.3_3D.geo #title: Cell 1.3_3D #messages: y

Figure 21 – B-scan of the total electric field obtained with GprMax2D for Cell 1.3 (finite-size concrete slab).
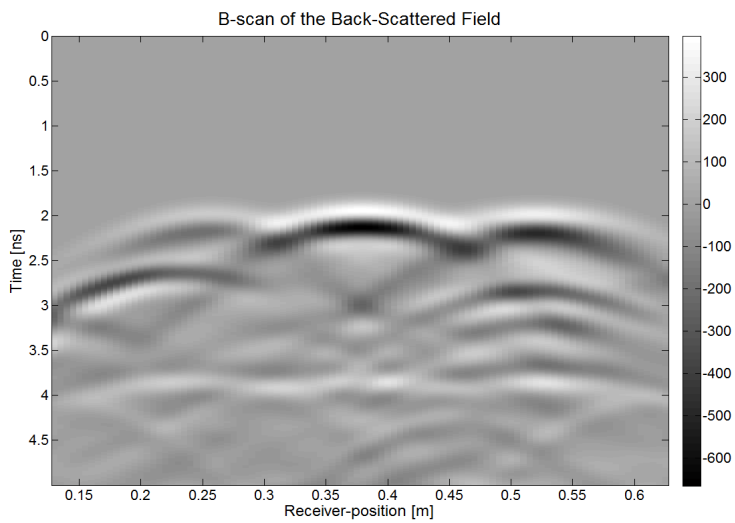

Figure 22 – B-scan of the back-scattered electric field obtained with GprMax2D for Cell 1.3 (finite-size concrete slab).
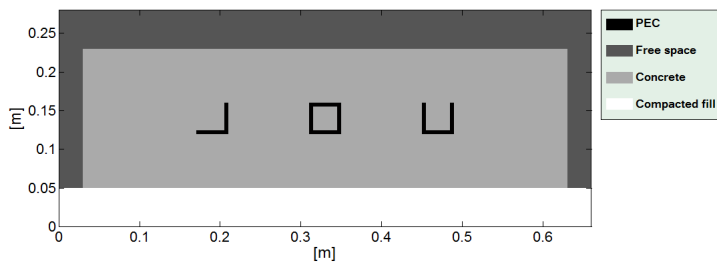
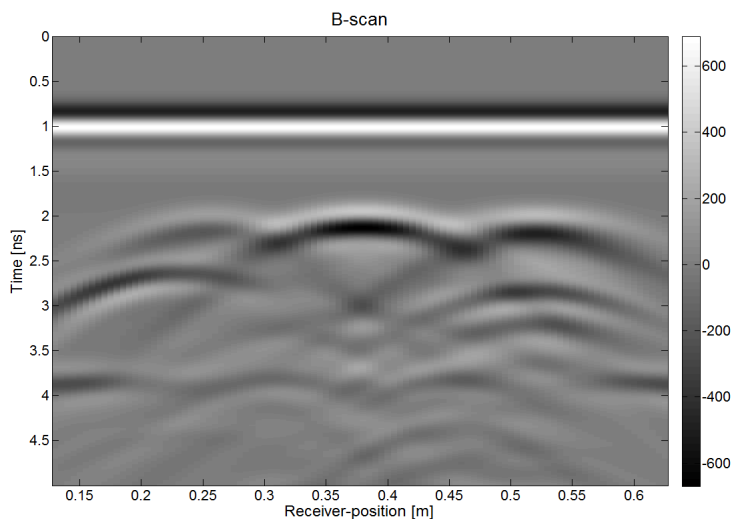Figure 23–Output geometry of Cell 1.3 (finite-size concrete slab).

Figure 24 – B-scan of the total electric field obtained with
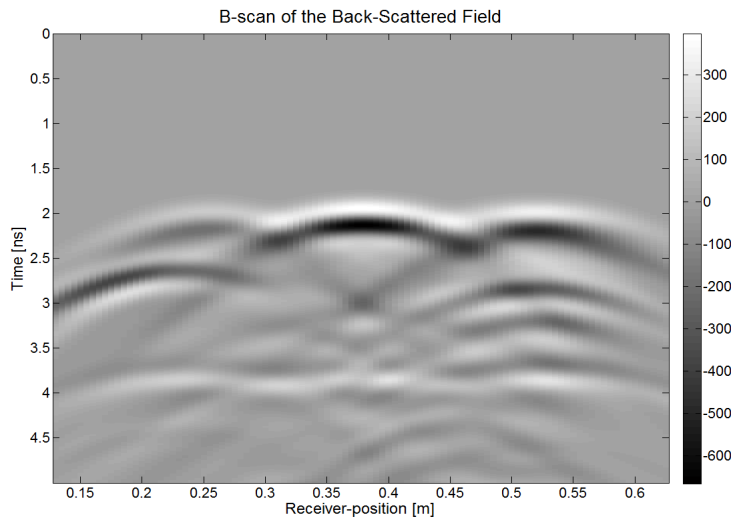GprMax2D for Cell 1.2 (infinite concrete slab).

41

Figure 25 – B-scan of the back-scattered electric field obtained with GprMax2D for Cell 1.3 (infinite concrete slab).

2.5: Interaction with COST Action TU1206

COST Action TU1206 "SUB-URBAN - A European network to improve understanding and use of the ground beneath our cities" focuses on the development of urban subsurface knowledge, its modeling, as well as the maximization of economic, social and environmental benefits of subsurface resources and ecosystem services. The possibility of organising a common workshop during Year 2 of the Actions' lifetime was discussed. Electromagnetic modelling of subsurface could be a topic of common interest. Further topics of common interest can be the application of GPR to locate artificial (man-made) and natural sub-superficial deposits, and the use of GPR in water management and protection.

3. FUTURE COLLABORATION WITH THE HOST INSTITUTION

Thanks to this STSM, a fruitful collaboration with the host institution has been established and will hopefully continue and grow.

- ❖ The simulation of concrete cells will be completed.

- ❖ Iraklis Giannakis (The University of Edinburgh, UK) is carrying out a STSM in "Roma Tre" University, on the numerical modelling of GPR antennas with the FDTD technique. Horn antennas as well as ridged horn antennas are being implemented to FDTD and their effectiveness is being tested in realistic modelled situations.

- ❖ Accurate models of the commercial antennas GSSI 1.5 GHz and MALA 1.2 GHz have been recently incorporated in GprMax: a comparison will be carried out, between GprMax results obtained for these antennas and results of commercial electromagnetic simulators as CST and HFSS, available in "Roma Tre" University.

- ❖ A further topic of future collaboration will be implementing in GprMax accurate models of soils as well as studying the effects of aggregates in the electromagnetic response of concrete. Stochastic methods can be used in order to realistically simulate the geometrical characteristics of both soils and concrete, advanced Debye approximations can be incorporated in order to simulate the real dielectric properties of the involved media in the frequency range of interest. Thanks to the possibility of accessing the cluster computer of The University of Edinburgh, it will be possible to execute large problems with high resolution (1 mm).

- ❖ Innovative ideas concerning the use of metamaterials in the design of GPR antennas and the miniaturisation of GPR antennas were discussed during the STSM carried out in

43

Edinburgh. In order to develop these ideas, a new project is starting in Working Group 1, focusing on the design, optimisation and modelling of GPR antennas and lead by Dr. Craig Warren (The University of Edinburgh, Edinburgh, UK).

4. FORESEEN PUBLICATIONS/ARTICLES RESULTING FROM THE STSM

The results of this STSM and of the ongoing STSM carried out by Iraklis Giannakis in "Roma Tre" University, will be presented during the 2014 European Geosciences Union General Assembly (2014 EGU GA):

- Lara Pajewski and Antonis Giannopoulos, "Electromagnetic modelling of Ground Penetrating Radar responses to complex targets," Geophysical Research Abstracts, Vol. 16, EGU2014-16421, 2014, EGU General Assembly 2014;
- Iraklis Giannakis, Antonis Giannopoulos, and Lara Pajewski, "Numerical Modelling of Ground Penetrating Radar Antennas," Geophysical Research Abstracts, Vol. 16, EGU2014-1553, 2014, EGU General Assembly 2014.

5. ACKNOWLEDGEMENTS

5. REFERENCES

[1] A. Giannopoulos, "Modelling ground penetrating radar by GprMax," Constr. Building Materials, vol. 19, pp. 755-762, 2005.
[2] K. S. Kunz and R. J. Luebbers, "The Finite Difference Time Domain Method for Electromagnetics," CRC Press, 1993.

[3]   A. Taflove, "Computational Electrodynamics: The Finite-Difference Time-Domain Method," Artech House, 1995.

[4]   K. S. Yee, "Numerical Solution of Initial Boundary Value Problems Involving Maxwell's Equations in Isotropic Media," IEEE Trans. on Antennas and Propagation, vol. 14, pp. 302-307, 1966.

[5]   A. Giannopoulos, "The investigation of Transmission-Line Matrix and Finite-Difference Time-Domain Methods for the Forward Problem of Ground Probing Radar," D.Phil thesis, Department of Electronics, University of York, UK, 1997.

[6]   J. H. Bungey, "Sub-surface radar testing of concrete: a review," Construction and Building Materials, 18, pp. 1–8.

[7]   R. Yelf and A. Ward, "Nine steps to concrete wisdom," Proc. 13th International Conference on Ground Penetrating Radar, Lecce, Italy, 21-25 June 2010, pp. 1-8.

[8]   T. Bourdi, J. E. Rhazi, F. Boone, and G. Ballivy, "Modelling dielectric-constant values of concrete: an aid to shielding effectiveness prediction and ground-penetrating radar wave technique interpretation," Phys. D: Appl. Phys. 45, Article ID 405401, 12 pp., 2012.

[9]   T. Bourdi, J. E. Rhazi, F. Boone, and G. Ballivy, "Application of Jonscher model for the characterization of the dielectric permittivity of concrete," J. Phys. D: Appl. Phys. 41, article ID 205410, 9 pp., 2008.

[10] T. Bourdi, F. Boone, J. E. Rhazi, and G. Ballivy, "Use of Joenscher model for estimating the thickness of a concrete slab by technical GPR," PIER M, Vol. 28, 89–99, 2013.

[11] C. Warren, A. Giannopoulos, "Creating FDTD models of commercial GPR antennas using Taguchi's optimisation method," Geophysics, 76, article ID G37, 2011.

STSM 2

THE PRESERVATION OF THE THOLOS TOMB OF ACHARNON

Visiting ESR: Dr. Sonia Santos Assuncao,
Polytechnic University of Catalonia, Barcelona, Spain

Host: Mr. Klisthenis Dimitriadis, Geoservice, Athens, Greece

STSM Dates: 15 January 2014 – 15 February 2014

1. PURPOSE OF THE STSM

During 2013 and at the beginning of 2014, an extensive geophysical survey was carried out and it is still ongoing in a very important Monument of the Hellenic Cultural Heritage, the Tholos Tomb of Acharnon. The geophysical survey was carried out from Geoservice under the supervision of Klisthenis Dimitriadis (geophysicist). The geophysical data acquisition has been assisted by Yannis Konstantakis (electronic engineer). Fotini Karassava (Architect) worked in close cooperation with Geoservice, from the beginning of this project. Two further organizations participate to this work in a form of partnership, and provide assistance. These are: the 2nd Ephorate of Prehistoric and Classical Antiquities of Greece, and the Municipality of Acharnon. The Ephorate is the responsible authority for the archaeological site as well as for all the ancient antiquities of Athens area and surroundings (except the Parthenon); its task is to protect and conserve the Antiquities in a sustainable way. The Municipality of Acharnon is the second in size municipality of the Attiki region, after the Municipality of Athens; its own interests are the preservation of the Acharnon Tomb and the touristic promotion of this monument to the maximum possible extent.

The STSM was carried out in Geoservice and had the main objective to study with Ground Penetrating Radar the Tomb of Acharnon. This monument has been built in the Mycenaean

period (1600 BC) and is characterised by a beehive shape with a circular base. Due to temperature and umidity variations, to vibrations produced both by the local traffic and the earthquakes, as well as to the high salt content of the unsaturated zone, there are several problems inherent to the preservation of the Tomb of Acharnon. In this STSM, the unknown thickness of the walls had to be determined; results were plotted using circular radargrams. Discontinuities in the radargrams may be associated to fissures or voids, indicating internal and external (superficial) damages of the Tomb, which are very important to be located and characterised. A combination of GPR with electrical resistivity tomography could allow us to perform a more accurate data interpretation. The vibrations in the Tomb could be quantified by using seismic measurements and the endoscopy was used to confirm the thickness of the building walls estimated by GPR. The host institution works with professionals from different scientific areas such as: geophysics, geochemistry, civil engineering, conservation and archaeology. A multidisciplinary team is essential to correctly interpret GPR radargrams.

2. DESCRIPTION OF THE WORK CARRIED OUT DURING THE STSM

Data acquisition was carried out in two areas of the Tomb: internal and external (i.e., the surface of the structure covering the Tomb). The internal part has been subdivided into three parts: i) the *dromos,* constituting the path to the Tomb, ii) the entrance, representing the connection between the *dromos* and the external part of the Tomb, and iii) the Tomb walls.

The STSM was principally focused to the study of the Tomb walls (iii), a structure characterised by 8.4 m diameter and 9 m height. Radar data were acquired and plotted in circular profiles.

The surfaces of the walls were extremely irregular. Hence, a thin polyurethane foam sheet was used to obtain a more regular surface in order to avoid noise as a consequence of the rough stone walls, see Figure 1, left part. This sheet also allows protecting the antenna from mechanical erosion. The effect of this thin extra-layer is not perceptible in radar images.

Profiles were marked on the walls with a laser. The antenna was moved along the line described by the laser, figure 1, right.

The complex structure required high coordination in the radar acquisition tasks, and a minimum of four persons were needed to execute properly all the process, adapting accurately the polyurethane sheet and assuring uniform motion of the radar antenna. A survey wheel provided the determination of the antenna position.

The height of the Tomb was 9 m. Therefore, the first 2 m could be studied without problems; the evaluation of the upper levels required the installation of scaffoldings. Three platforms divided the total volume in four parts (level 0, 1, 2 and 3), allowing the access to entire wall.

Three different center frequency antennas were used in the study. The inner part of the Tomb was evaluated by means of a 1 GHz center frequency antenna, obtaining enough resolution to image the walls until 1 m of thickness.

Figure 1 – Data acquisition. Left: Sample of the anomalous surface with a fissure. Right: Laser to produce the circular profiles.

In the exterior of the Tomb, a 500 MHz center frequency antenna was used, to study the material covering the Tomb. Finally, a 2.3 GHz center frequency antenna was employed to

analyze the radar wave velocity that was used to convert two-way travel times into depths.

3. Description of the main results obtained during the STSM

An accurate analysis of the radar data allowed us to define the existence of two irregular layers of stones that constitute the walls of the Tomb. The main anomalies are caused by discontinuities in the materials. An average thickness could be determined, although it was highly variable. Figure 2 shows the radar image over one meter; this data are extracted from a circular profile. Figure 3 shows the whole circular radargram, taking into account and representing the geometry of the Tomb. Both figures illustrate the existence of layers, irregular targets and discontinuities associated to cracks, fissures and voids. High attenuation was present in several areas. This effect was caused by the presence of salt.

In the circular radargrams, reported in Figure 3, it is possible to appreciate the thickness of the wall and the discontinuities of internal layers to be associated with fissures and voids. Due to localized signal attenuation and presence of salts detected by visual inspection, it is also possible to map zones with higher salt content. The three dimensional model, resulting from the interpolation of GPR profiles collected at different heights, provides an estimation of the real shape of the anomalies as well as the possibility to analyze their vertical continuity.

The GPR data are in accordance with the results of the micro-resistivity surveys carried out in a second phase of the study. This additional geophysical method used ERT (Electrical Resistivity Tomography) to map the walls in profiles of 3.1 m. This allowed us to verify the interface between the wall of the grave (schist stones) and his geological environment (very fine sand). In Figure 4, a characteristic profile is presented. Low resistivity correspond to sand and high resistivity (red areas) to the wall of the grave.
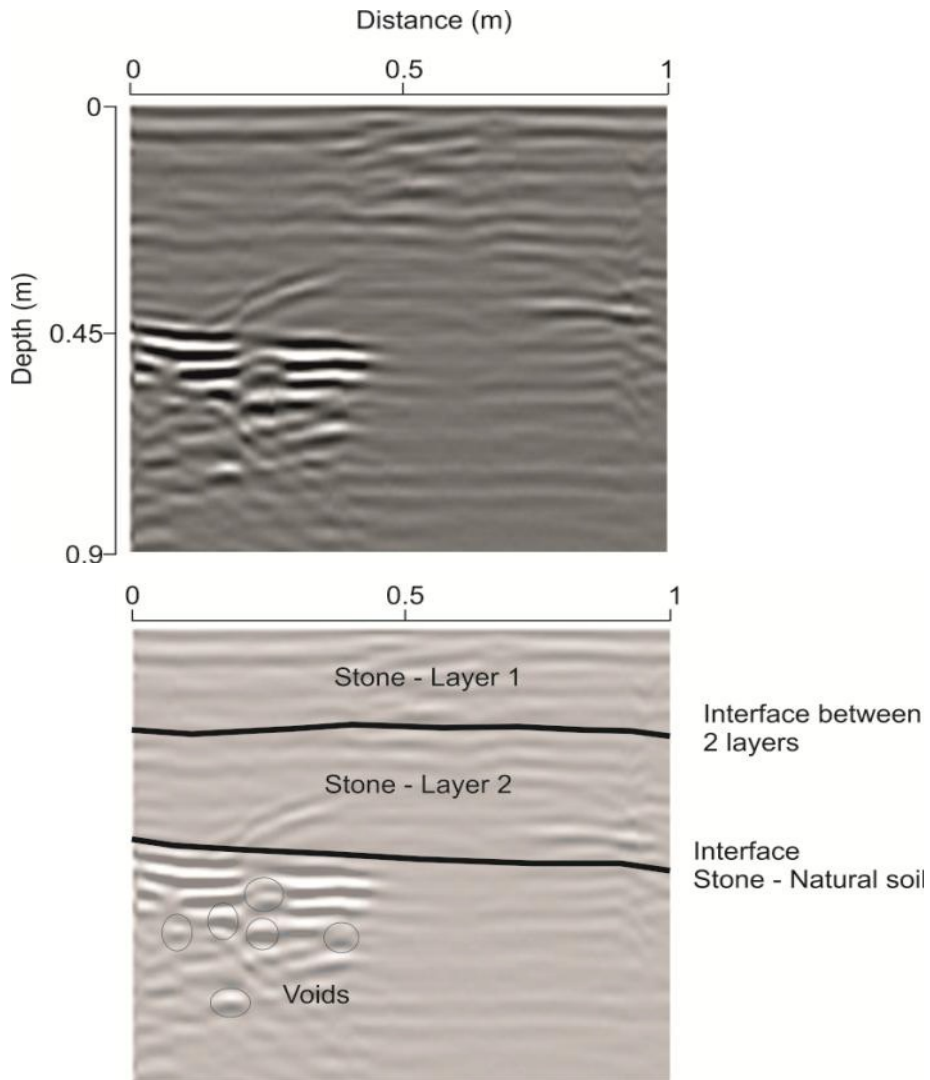
Figure 2 - Profile measured at 23 cm height. Up – Filtered radargram; Down – Interpreted radargram.
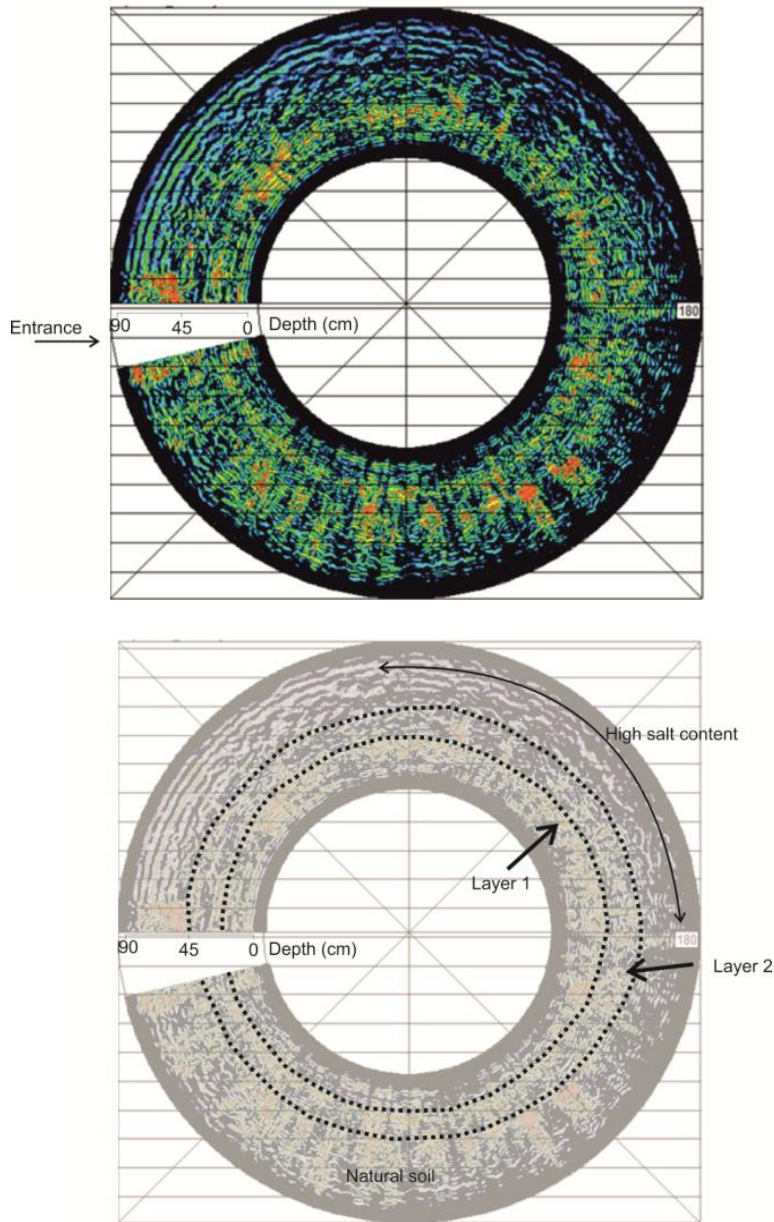
Figure 3 - Profile measured at 23 cm of height, depicted in circular shape, respecting the entrance size. Up – Filtered radargram; Down – Interpreted radargram.
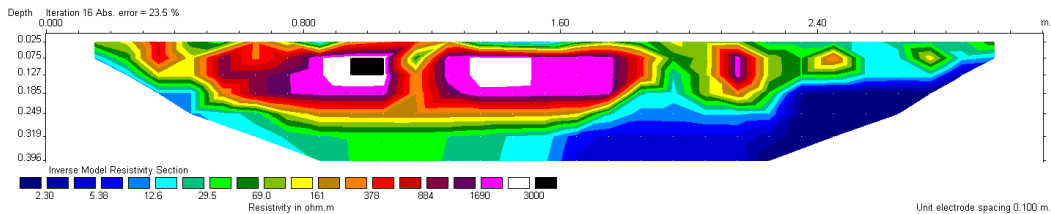
Figure 4- Electrical resistivity tomography.

4. FUTURE COLLABORATION WITH THE HOST INSTITUTION

Given the results obtained in Tomb of Acharnon, the methodology used to analyze the Tomb of Acharnon could be standardized. In this way, this procedure cOULD be applied to other archaeological monuments.

The circular GPR technology is of great interest for the host institution, especially to carry out investigations of Ancient columns, mostly made of marble or sandstone, in order to map stone imperfections or internal cracks and deterioration.

5. FORESEEN PUBLICATIONS/ARTICLES RESULTING FROM THE STSM

ThIS work will be presented during the 2014 European Geosciences Union General Assembly (2014 EGU GA):

➢ Sonia Santos Assuncao, Klisthenis Dimitriadis, Yannis Konstantakis, Vega Perez-Gracia, Eirini Anagnostopoulou, Mercedes Solla and Henrique Lorenzo, "Non-destructive assessment of the Ancient Tholos Acharnon Tomb building geometry, Geophysical Research Abstracts, Vol. 16, EGU2014-13961-1, 2014, EGU General Assembly 2014.

6. ACKNOWLEDGMENTS

The interdisciplinary team working on the non-destructive assessment of the Tholos Tomb of Acharnon, during the STSM

STSM 3
NUMERICAL MODELLING OF GROUND PENETRATING RADAR ANTENNAS

Visiting Researcher: Mr. Iraklis Giannakis
The University of Edinburgh, Edinburgh, United Kingdom

Host: Dr. Lara Pajewski, Roma Tre University, Rome, Italy

STSM Dates: 22 January 2014 – 22 March 2014

1. PURPOSE OF THE STSM

Realistic and effective ground penetrating radar (GPR) modelling is based on efficient and accurate solutions of Maxwell's equations. Numerical methods for solving Maxwell's equations range from finite element methods, the method of moments, finite difference implicit techniques, transmission-line matrix (TLM) methods and others (Sadiku, 2000). One of the most highly used methods however is the finite difference time domain (FDTD). The reasons for its popularity are its simplicity and computational efficiency (Taflove, 2000).

GprMax (Giannopoulos, 2005) is a freely available GPR modelling software package, which solves Maxwell's equations and is used throughout this paper. GprMax employs a second order in both space and time FDTD algorithm first described by Yee (1966).

GPR numerical modelling has been widely used to study and enhance data understanding and interpretation in a variety of GPR applications. Amongst them, dense non-aqueous phase liquids (DNAPL) detection (Wilson et. al. 2007), tunnel inspections (Xianqi et. al. 2009), bridges evaluation (Diamanti et. al. 2011), forensic applications (Hannon et. al. 2000), landmine detection (Oguz and Gurel 2000). For near surface applications however, like forensic, engineering and landmine detection, the scale of the problem and the proximity of targets to GPR sensors gives rise to some unique characteristics which must be taken into account for

realistic and effective GPR modelling. Two of the most important of these characteristics are:

- The antenna occupies a relative large volume in the modelled domain, this means that the antenna is not only related to the characteristics of the transmitted pulse (directivity, central frequency etc.) but also is part of the model, which contributes to the measured scattered field.
- Increased sensitivity to background characteristics due to the high frequency content of the pulse, this means that media inhomogeneity and rough surfaces must be included into the model.

A numerical pavement-evaluation case study is presented in this report, to illustrate the developed modelling framework.

Pavement evaluation traditionally requires the retrieval of information about the layer thickness within the pavement as well as the dielectric properties of the latter. Air-coupled horn antennas are often used for this purpose. The main drawbacks of horn antennas are their low spatial resolution and their inability to often illustrate clear hyperbolic scattering phenomena (Diamanti, 2012). The mentioned drawbacks create doubts about the effectiveness of air-coupled antennas in detecting lateral cracks within the pavement.

In our simulations, pavement is realistically modeled. Fractals are used to mathematically define the stochastic variation of the dielectric properties within the pavement as well as its rough surface. Two different antennas, one air-coupled horn antenna and one ground-coupled bowtie, are implemented into the model and their effectiveness in pavement evaluation and crack detection is compared.

The main aim is to present and establish a realistic modeling framework that can be used in evaluating antenna designs and their performance in complex near surface GPR investigations.

2. DESCRIPTION OF THE WORK CARRIED OUT DURING THE STSM

Air coupled antennas like horn antennas have been extensively used for pavement evaluation using Ground Penetrating Radar (GPR). The main reasons for that are:

- They are capable to detect thin layers.
- They operate safely in highway speeds because they don't need to be close to the ground.
- They are relative easy to manufacture.

We examine an E-plane monostatic horn antenna with central frequency of 2.6 GHz.

Regarding the feeding of the antenna, a TE10 mode is used which is excited inside a rectangular waveguide with dimensions 0.25 x 0.022 m. With the previously mentioned dimensions, a single mode of propagation in the frequency range 0.6 – 6.8 GHz is achieved. The receiver is modeled by a coaxial cable. The inner and outer conductor of the coaxial cable have radii of 0.5 mm and 4 mm respectively and it is filled with plastic with relative electrical permittivity equal to 2.5. The spatial discretization step of the model is $\Delta l = 1$ mm and the time step is equal with $\Delta t = 1.925$ ps (Courant limit). Figures 1 and 2 illustrate the geometry of the antenna and the propagation of the TE10 mode inside it.

Apart from the horn antenna described above, a ground coupled bowtie antenna is also implemented into the models (Figure 3). The model of this antenna is based on a commercial available antenna, which is designed for near surface applications as introduced by Warren and Giannopoulos 2011.

The previously described antennas are tested in a realistic pavement evaluation scenario. The pavement consists of two layers, the asphalt layer and the base as depicted in Figure 4.
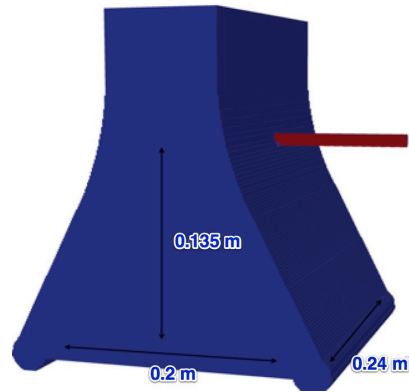
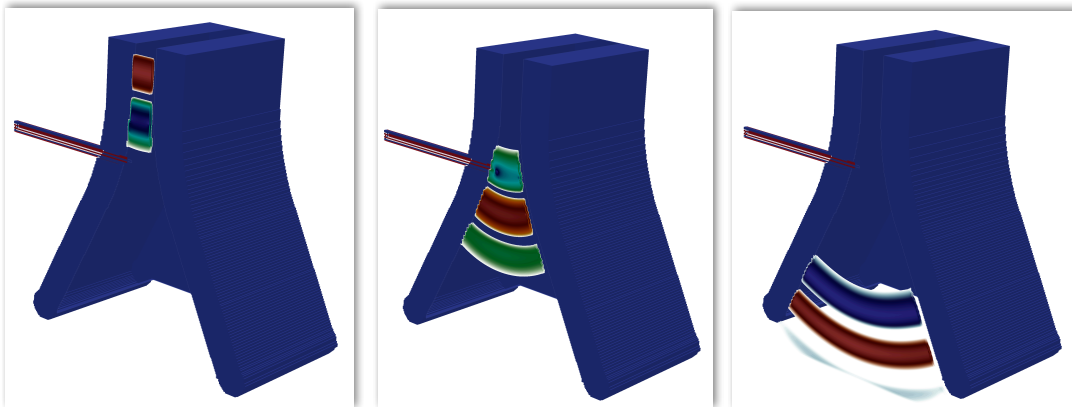Figure 1 - The geometry of the 2.6 GHz monostatic horn antenna.

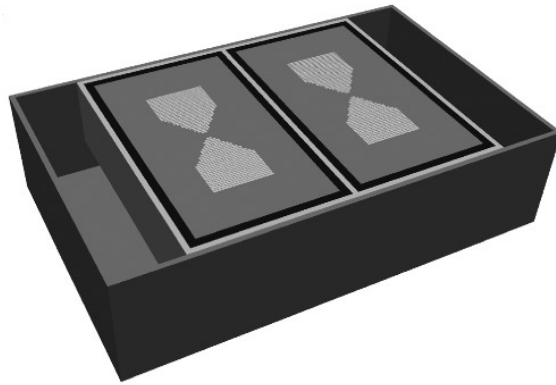Figure 2 - Snapshots of the TE10 mode propagating inside the horn antenna.

57

Figure 3 - Ground coupled bowtie antenna
with central frequency of 1.6 GHz.

The asphalt layer has a relative electric permittivity, which varies stochastically from 6 to 8 and the base from 10 to 12. The conductivity of both layers is equal to σ =0.01 S/m. Fractals were used in order to create realistic variations of the dielectric properties within each layer. The pavement's surface is relatively smooth with small variations as it is expected in old or highly used roads. Again fractals were used to incorporate the rough surface. Three cracks created using random walks are implemented into the model. The cracks are filled with air and they have a 3 mm width. One of them occurs in the first layer but does not reach the surface, another one occurs in the second layer and the third one cuts through both layers. The dimensions of the model (x, y, z) are 1300 x 300 x 600 mm. The simulations were executed in a parallel computing environment using the cluster computer provided by The University of Edinburgh. In order to reduce the computational cost, we divide the domain in subdomains according to the position of the antenna unit. Every trace of the resulting B-scan is as a result calculated in a different subdomain. Using this scheme we have assumed that the scattering field that might exist outside of the subdomains is negligible compared with the scattering field inside the subdomain.

The horn antenna is placed at 20 cm above the ground while the bowtie antenna is placed 2 cm above the ground. Figure 5 illustrates the resulting B-scans from both antennas. A linear gain is applied to the resulting B-scan using the horn antenna. From Figure 5 (left side) is evident that clear reflections from the base are obtained and the cracks practically do not contribute to the received scattering field.Using the bowtie antenna and a singular value decomposition (Kim et. al. 2000) results to the B-scans shown in Figure 5 (right side). From the B-scans it is evident that all the cracks give clearer and more prominent interpretable hyperbolic responses.
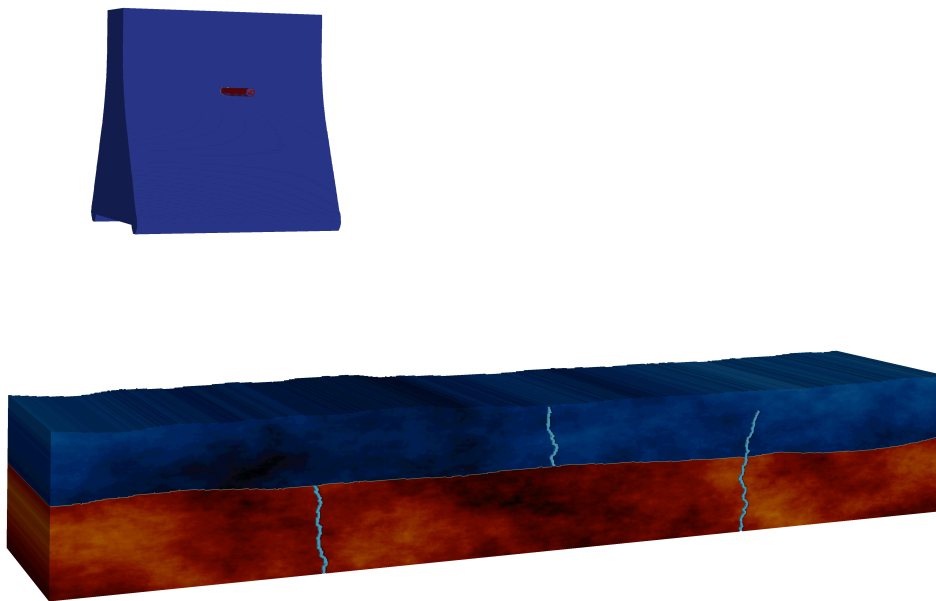
Figure 4 - The modelled pavement evaluation scenario. The medium is consisted with two non-homogenous layers and three air-filled cracks are also included into the model.
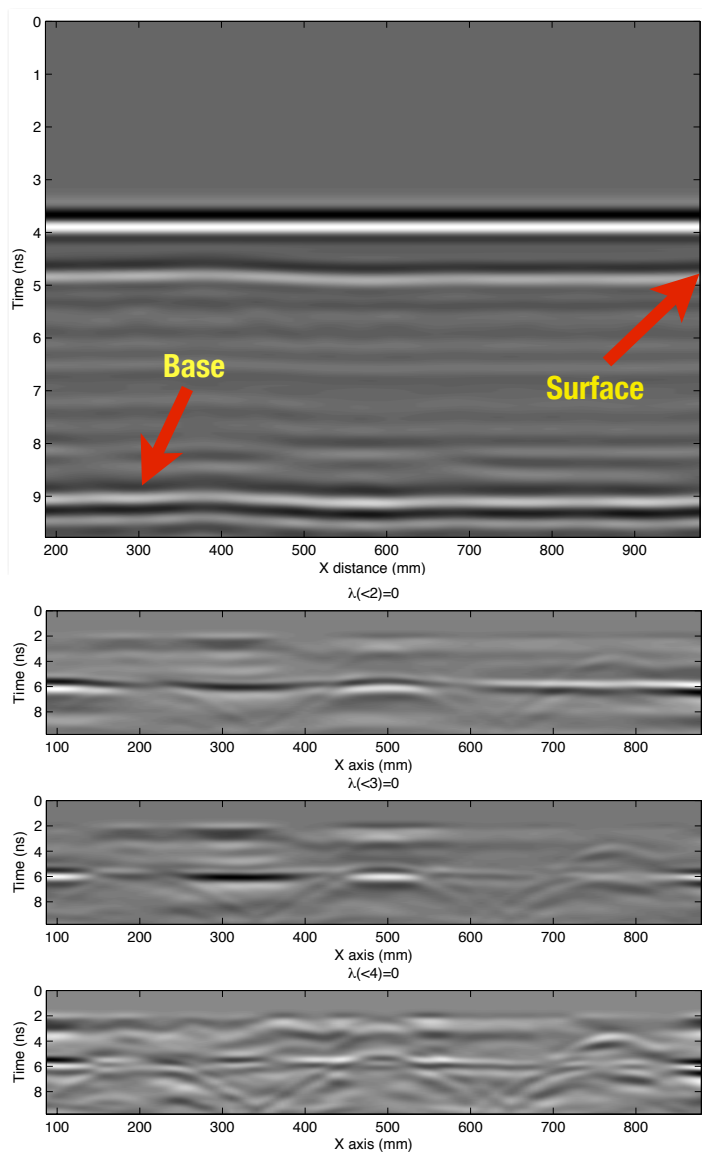
Figure 5 - Left: The resulting B-scan (after linear gain) using the air-coupled 2.6 GHz horn antenna. Right: The B-scans using the ground coupled bowtie antenna, after removing 2,3 and 4 dominant eigenvalues.

3. DESCRIPTION OF THE MAIN RESULTS OBTAINED DURING THE STSM

An air-coupled horn antenna and a ground-coupled bowtie antenna are tested in a realistically modeled pavement evaluation scenario. The numerical results indicate that air-coupled antennas receive clear reflections from distinct layers within the pavement but they are incapable in this setting to detect cracks filled with air. On the other hand, using ground-coupled antennas results to clear and easy to interpret hyperbolic responses from the buried cracks. The developed modeling framework is a powerful tool in evaluating the performance of high frequency GPR transducers in realistic situations and this approach can lead to better design of GPR antennas.

4. FUTURE COLLABORATION WITH THE HOST INSTITUTION

Air coupled antennas are a very practical choice for pavement evaluation due to their ability to operate on highway speeds. The research done so far suggest that air coupled antennas like horn antennas are not effective when it comes to air filled crack detection. Future work will include the design of a novel air couples antenna which will be able to reliable detect air filled cracks.

Future work also includes modeling of generic type of GPR antennas and assessing their performance in more case civil engineering applications.

5. FORESEEN PUBLICATIONS/ARTICLES RESULTING FROM THE STSM

The STSM work will be presented during the 2014 EGU General Assembly:

> ➢ I. Giannakis, A. Giannopoulos, L. Pajewski, "Ground Penetrating Radar Antennas", Geophysical Research Abstracts, vol. 16, EGU 2014-1553, 2014.

6. ACKNOWLEDGMENTS

7. REFERENCES

Diamanti N. and Redman D., 2012, Field observations and numerical models of GPR response from vertical pavement cracks, Journal of Applied Geophysics, vol. 81 pp. 106-116.

Diamanti N. and Giannopoulos A., 2011, Employing ADI-FDTD subgrids for GPR numerical modelling and their application to study ring separation in brick masonry arch bridges, Near Surface Geophysics vol. 9, pp. 245-256.

Giannopoulos A, 2005, Modelling of ground penetrating radar using GprMax, Construction and Building Materials, vol. 19, No 10, pp. 755 – 762.

Hammon W.S, McMechan G.A and Zeng X., 2000, Forensic GOR: finite- difference simulations of responses from buried human remains, Journal of Applied Geophysics, vol. 45, pp. 171-186.

Kim J. H, Cho S. J. and Yi M. J, 2007, Removal of ringing noise in GPR data by signal processing, Geosciences Journal, vol. 11, pp. 75-81.

Sadiku M.N.O., 2000, Numerical Techniques in Electromagnetics, Second edition, CRC press.

Oguz U. and Gurel L., 2002, Frequency responses of ground-penetrating radars operating over highly lossy grounds, IEEE Trans. Geosci. Remote Sensing, vol. 40, no. 6, pp. 1385-1394.

Taflove A. and Hagness S. C., 2000, Computational Electrodynamics, The Finite-Difference Time-Domain Method, 2nd ed. Norwood, MA: Artech House.

Warren C. and Giannopoulos A., 2011, Creating FDTD models of commercial GPR antennas using Taguchis optimisation method, Geophysics, vol. 76, no. 37.

Wilson V., Power C., Giannopoulos A., Gerhard J. and Grant G., 2009, DNAPL mapping by ground penetrating radar examined via numerical simulation, Journal of Applied Geophysics, vol. 69, pp. 140-149.

Xianqi H., Ziqiang Z., Guangyin L. and Qunyi L., 2009, The FDTD Modeling of GPR for Tunnel Inspection, International Conference on Information Engineering and Computer Science, pp.1-4.

Yee K. S., 1966, Numerical Solution of Initial Boundary Value Problems Involving Maxwell's Equations in Isotropic Media, IEEE Trans. Antennas Propag., vo. 14, pp. 302-307.

STSM 4

**RECONSTRUCTING PREHISTORIC ENVIRONMENTS AT STONEHENGE
WITH MULTIPLE ELECTROMAGNETIC SURVEY METHODS**

Visiting ESR: Mr Philippe De Smedt,
Ghent University, Ghent, Belgium

Host: Dr Immo Trinks, Ludwig Boltzmann Institute for
Archaeological Prospection and Virtual Archaeology,
Vienna, Austria

STSM Dates: 1 February 2014 – 31 March 2014

1. PURPOSE OF THE STSM

The rationale of this project is that by mapping electromagnetic soil properties using different near surface geophysical survey methods an integral reconstruction can be attempted of the variations caused by anthropological, pedological and geomorphological structures in the subsurface. In order to achieve this, datasets from different multichannel GPR and electromagnetic survey systems will be compared and jointly interpreted. The different datasets that were processed, analysed and compared were data from 1) a multi-receiver electromagnetic induction (EMI) survey, and 2) a 3D ground-penetrating (GPR) survey collected. The EMI data were collected in 2012 by the Research Group Soil Spatial Inventory Techniques (ORBit) from Ghent University (Belgium), while the GPR data were gathered by the Ludwig Boltzmann Institute for Virtual Archaeology and Archaeological Prospection (LBI ArchPro) from Vienna (Austria).

The multi-receiver EMI data were collected with a Dualem-21s sensor that records the soil apparent electrical conductivity (ECa) and the apparent magnetic susceptibility (MSa) data of four different soil volumes simultaneously. The sensor consists of 1 transmitter and four receiver coils spaced 1 m, 1.1 m, 2 m and 2.1 m apart. The receiver coils at 1 m and 2 m from the transmitter are placed in horizontal coplanar mode (1 m and 2 m HCP

respectively), while those at 1.1 m and 2.1 m are placed in perpendicular mode (1.1 m PRP and 2.2 m PRP respectively). This results in penetration depths down to 0.5 m, 1 m, 1.5 m and 3.2 m below the surface for the ECa data. Further information on the Dualem-21s sensor can be found in (Saey et al., 2009). The multi-layered dataset offers insight into the vertical and lateral variations in ECa and MSa and can serve as a basis for the 3D reconstruction of subsurface variations (e.g. Saey et al 2008, De Smedt et al. 2013).

The 3D GPR data, gathered with a MALÅ Imaging Radar Array (MIRA) system in motorized configuration, provides information on the soil dielectric permittivity and on soil discontinuities in 3D. This MIRA system consists of 16×400 MHz channels with 0.08 m cross-line channel spacing and possibilities for 0.04 m or 0.08 m in-line GPR trace spacing.

During the research stay we aimed at creating a robust methodological foundation for the combined analysis of the EMI and GPR data on which we can build future work and research combining these two methods.

2. Description of the work carried out during the STSM

During the research stay at the LBI ArchPro, EMI data gathered at Stonehenge were processed to allow combination with the GPR data. The different available GPR datasets of the study area were simultaneously analyzed, and an area was selected where the EMI and GPR datasets would be jointly analysed and combined (Fig. 1). This specific area was selected as 1) it holds clearly defined remains of a prehistoric monument (Fig. 2a), which was interpreted as a segmented ditch, 2) a number of geomorphological variations were observed in the EMI data (a palaeoriver (Fig. 2b) and variations in the chalk bedrock morphology (Fig. 2c). A comparison between the different geophysical datasets in this area would allow addressing the main research questions; i.e. a better understanding of the anthropological, pedological and geomorphological variations within the Stonehenge World Heritage Site.

The main research effort during the STSM was directed towards a better understanding of the pedology and geomorphology of the study area through the combined analysis of GPR and EMI data.

As a starting point, geostatistical analyses were performed on the EMI data to extract only variations that could be attributed to the morphology of the chalk bedrock. For this, ECa data from the 2.1 m PRP coil configuration (Fig. 2, left) were deemed the most suited as the depth sensitivity of these measurements accords with the depth range of the targeted soil variation (i.e. between 0-1 m below surface (Fig. 4). These slices were produced through in-house developed software from the LBI ArchPro institute.
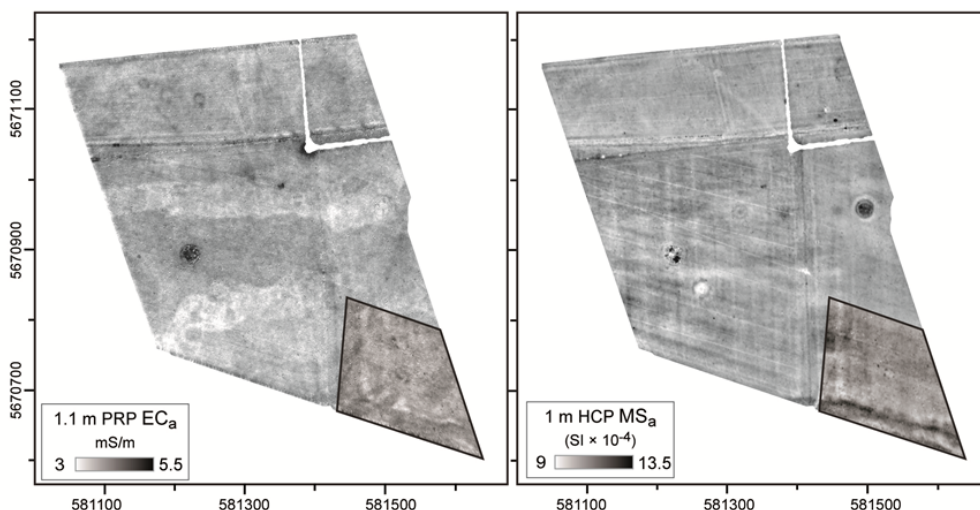
Figure 1 - Plot of the 1.1m PRP ECa data (left) and the 1 m HCP MSa data (right) from the 2012 EMI survey area. The subzone that was selected for detailed analysis during the STSM is highlighted and bordered by a black line in both plots.
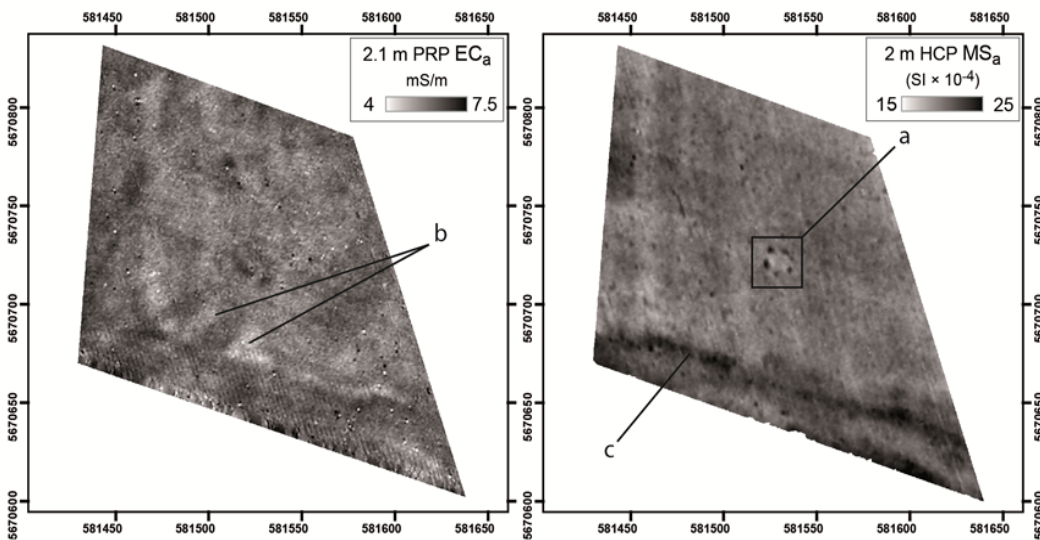
Figure 2 - Detail of the EMI data from the subzone indicated in Fig. 1. Left: 2.1 m PRP ECa data with indication of a low conductive area that is attributed to shallow chalk beneath the more conductive soil. Right: 2 m HCP MSa data with indication of the prehistoric monument (a) that is visible as a segmented ditch, and indication of the increased magnetic susceptibility that is attributed to palaeochannel sediments.

After these datasets were produced, areas were selected where a significant overlap could be found between strong reflections in the GPR data on the one hand, and shallow bedrock as located through the classified ECa data. At these locations the preliminary depths, as extracted from the GPR profiles and depth slices where compared to the ECa data values from all coil pairs from the Dualem-21s sensor. Following the procedure of Saey et al. 2008 and De Smedt et al. 2011, these depths were then used as calibration values to model the depth of the chalk bedrock based on the ECa data.
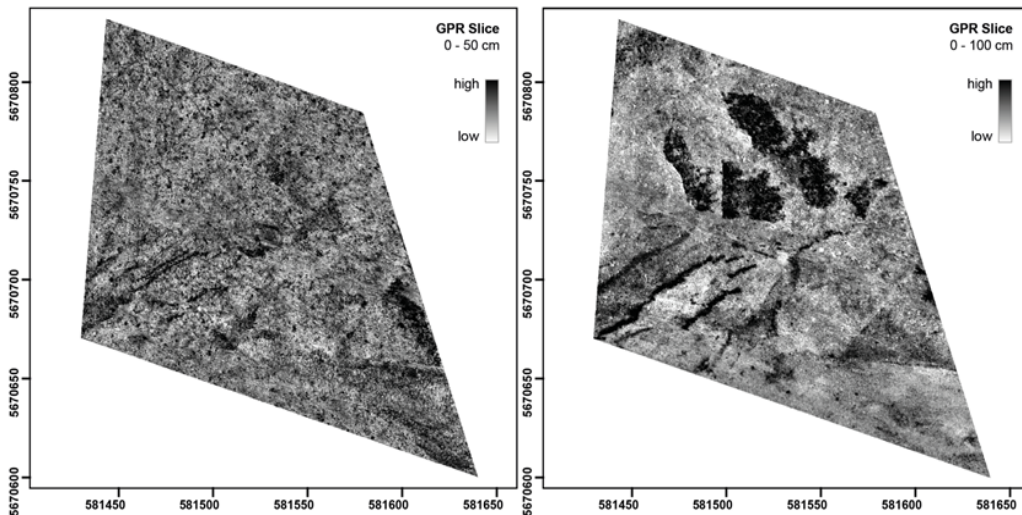
Figure 3 - GPR depth slices representative for a depth range of 0-0.5 m below the surface (left) and for a range of 0-1 m below the surface (right).

The second research topic that was addressed, focused on the archaeological variations within the study area. Again geostatistical data analyses were used as a starting point. The main datasets that were used were the MSa data from the 1 m and 2 m HCP coil configurations (Fig. 1 and 2, right), and the 0-0.5 m GPR depth slice (Fig. 3, left). Principal component analysis was conducted in Isatis to visualize the small scale variation present within these datasets within the study area. In a final step, the results of the first and second research topics were combined to allow a fuller interpretation of the subsurface variation within the study area.

3. DESCRIPTION OF THE MAIN RESULTS OBTAINED DURING THE STSM

Analysis of the 2.1 m PRP data showed a distinct large scale spatial variation that could be clearly visualized through isolating

the relevant spatial structural component with factorial kriging (Fig. 4, left). The resulting data were then successfully classified through fuzzy k means classification, offering a detailed map of the geomorphological variation that was detected through the EMI survey (Fig. 4, right).
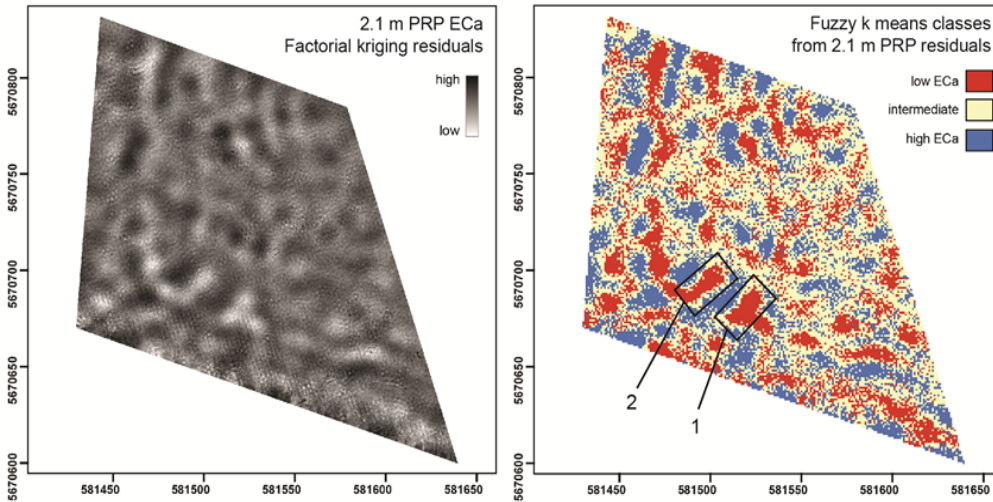

Fig. 4: Left: Residual 2.1 m PRP ECa data produced through factorial kriging analysis, representing the large scale spatial variation within the study area. Right: Classified residual 2.1 m PRP ECa data. The low ECa data (red) class can be interpreted as shallow chalk bedrock, while the high ECa data class (blue) represents deeper bedrock (i.e. thicker overlaying soil layer). The areas indicated with 1 and 2 are those were the best visual correlation was found with high reflections in the GPR depth slice.

Visual comparison between the high reflections in the 0-0.5 m GPR depth slice (Fig. 3) and the areas with shallow chalk as present in the classified EMI ECa data, allowed identifying two zones where a direct correlation could be witnessed between these datasets (1 and 2 on Fig. 4).

We attempted to correlate these structures to specific reflections in the separate GPR profiles, but were unable to do so in a robust manner during the STSM. The correlation was only possible based on the visual analysis of the 0.5 m thick GPR slice and of 0.05 m thick slices within the 0 – 0.5 m depth range. We found that only at specific locations the GPR reflections could be correlated to the depth of the interface between the soil and the underlying chalk bedrock. It was therefore proposed that the boundary between soil and bedrock was often characterized by a gradual transition between the weathered soil material and the underlying chalk. While the difference in electrical conductivity allows discerning between these two layers (i.e. soil and chalk), these do not represent discontinuities that are easily identified in the non-migrated GPR data. The largest reflections in the GPR data are produced by discontinuities present within the chalk bedrock (e.g. fractures and intercalated flint patches) (Fig. 5).

To model morphology of the chalk bedrock, we therefore introduced preliminary depths into the modeling procedure based on the correspondence between the 0.05 m thick GPR slices and the EMI classification. This way, we were able to generate a preliminary model of the bedrock morphology (Fig. 6). The resulting model shows a different morphology than the smooth current topography.

In a following step the comparison of the MSa data and the GPR data was taken on. After resampling the data to the same grid, PCA of the different datasets were conducted. It was found that the correlations between them were not significant (i.e. $r < 0.1$) to provide a basis for detailed interpretation of the detected variations (a problem which was equally observed by Kvamme (2006) when combining multiple geophysical datasets for archaeological interpretation). However, visualizing the first component loadings of the PCA of the full 2 m HCP MSa dataset and the 0.5 m thick GPR slice, did offer a straightforward insight into the features that contribute the most to the combined variance within the study area. While the resulting data offer no basis for quantitative analysis or characterization of the detected

70

features, these do facilitate the visual evaluation of the small scale variation present within both datasets.

The features indicated on Fig. 7 represent the clearest and most characteristic anomalies that were found through the evaluation of the combined data plot. In the center of the area, a prehistoric monument is present that was most visible in the MSa data. Southwest of the segmented ditch, a strong reflection can be seen leading up to this monument. Adjacent this reflection, the bedrock model reveals small depressions that are possibly man-made.
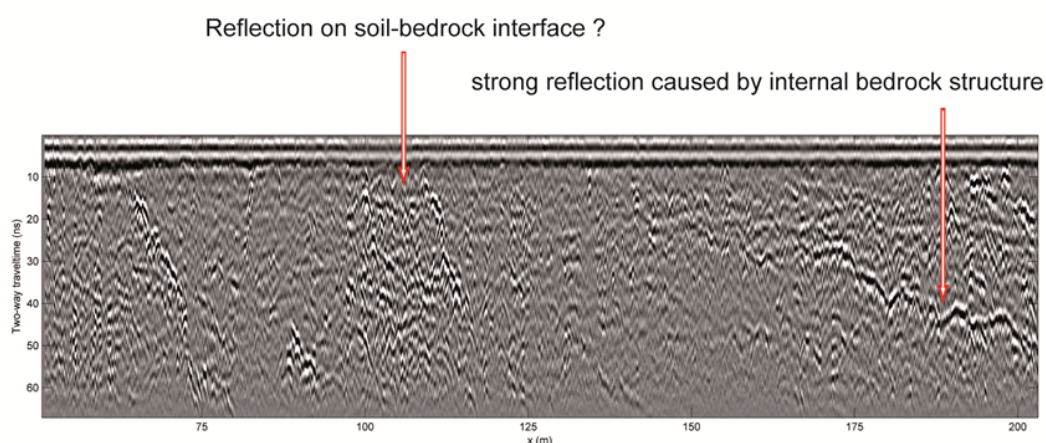
Fig. 5: GPR profile over a location where shallow chalk was suggested by the EMI data analysis (see Fig. 4). The location where shallow bedrock was assumed is indicated (left arrow) along with a characteristic deeper GPR reflection as present throughout the entire dataset (right arrow).

71
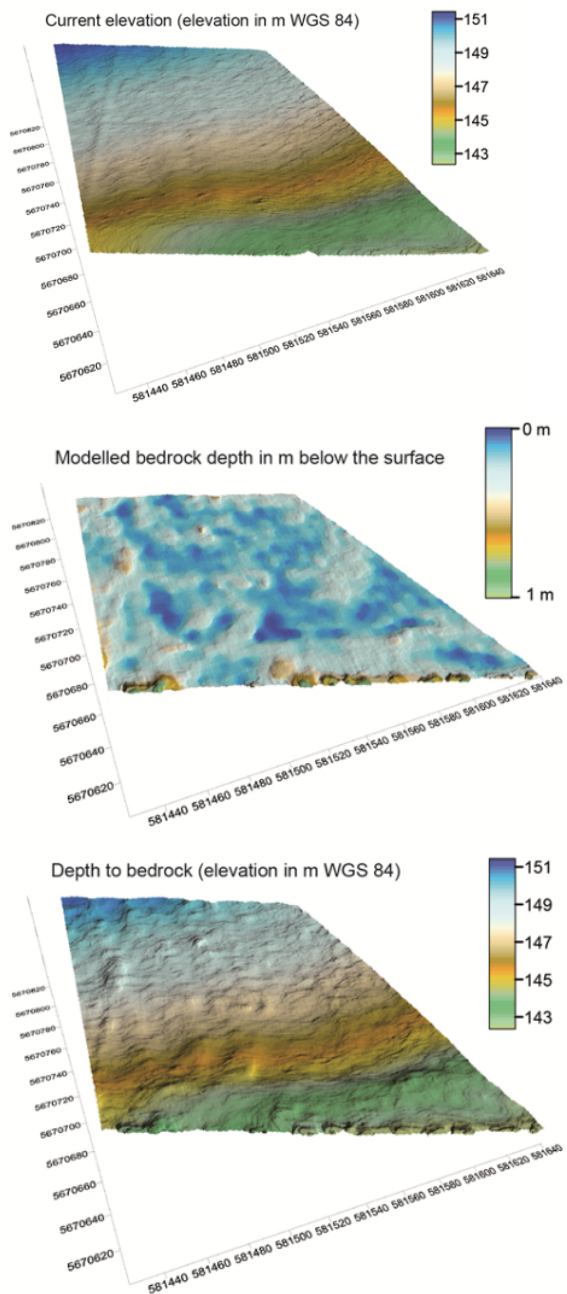
Figure 6 - Combined 3D data plot showing the bedrock model with overlay of the 1st component loadings of the MSa – GPR principle component analysis with indication of the most characteristic features.

Farther to the edge of the area we find another, larger depression in the bedrock that leads from the palaeochannel deposits in the far south(west) of the area and directs towards the monument. This depression is flanked by two linear expressions of shallow bedrock, present in both the GPR and ECa data.

The presented results show the potential of combining EMI and GPR for detecting and characterizing different types of subsurface variations at Stonehenge. While during the research stay the results have been mainly descriptive, we did however lay out a methodological work flow for a quantitative combination of the different datasets.

4. FUTURE COLLABORATION WITH THE HOST INSTITUTION

We are currently already advancing the work that was started during the STSM. To further the modelling of the calcareous bedrock, we are reprocessing the GPR data. This work is being done in close collaboration with the LBI ArchPro (more specifically with Eng. Alois Hinterleitner and Dr. Immo Trinks), dr. Lieven Verdonck (Dept. of archaeology, Ghent University) and the ORBit research group from Ghent University. To date we have successfully migrated the GPR data, offering a more accurate insight into the true depth of the detected features. This is also allowing to better discern the interface between the soil and the underlying bedrock (Fig. 7).

In a following step we will conduct a correlation analysis between the migrated GPR data and the ECa data (see above) to establish a calibration dataset and build a bedrock model with increased accuracy.

Based on the further processing and analysis of the GPR data, we plan to investigate the relationship between the MSa data and the small scale anomalies present in the GPR data. Here as well, the migration of the GPR data should provide a rigorous basis for a more robust comparison of these two data types.

While this was not elaborated on during the STSM, we have started comparing the MSa data to the magnetometry data from the LBI ArchPro. These data were exchanged during the research

stay and we are pursuing a combination of these two datasets to better characterize the nature of magnetic variations within the study area (e.g. discerning between recent metal debris and relevant archaeological variations within the study area).
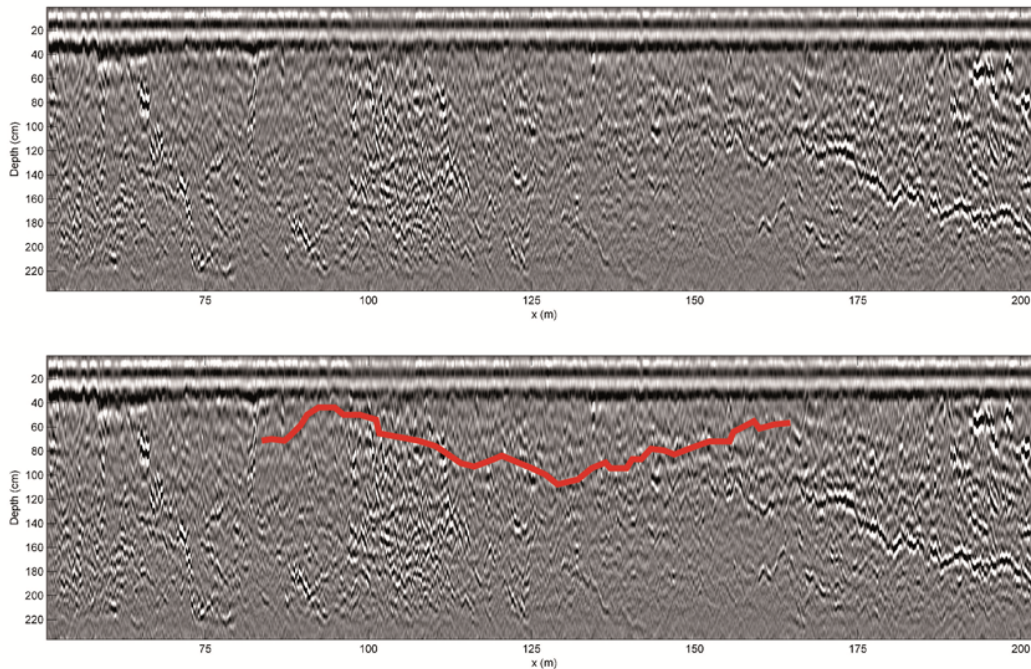

Figure 7 - Migrated GPR profile (similar as the non-migrated data presented in Fig. 5). Both profiles in the illustration show the same data, in the bottom illustration a minute reflection is traced that was (preliminary) attributed to the interface between the soil and the underlying bedrock. Migration procedure and illustration are courtesy of dr. Lieven Verdonck.

5. FORESEEN PUBLICATIONS/ARTICLES RESULTING FROM THE STSM

We aim at a publication on the joint use of 3D GPR data and multi-receiver EMI (ECa) data to model the depth to a pre-defined soil layer at Stonehenge. The model results presented in this report are a prelude to this work, and the reprocessing of the GPR data discussed above are providing the basis for a more quantitative data integration needed for such a publication.

The combined analysis of the MSa and magnetometry data is also aimed towards at least one publication. This work mainly focusses on differentiating between recent and archaeological soil intrusions.

6. ACKNOWLEDGMENTS

7. REFERENCES

De Gruijter, J. J. & McBratney, A. B. 1988. A modified fuzzy k-means method for predictive classification. In: Classification and Related Methods of Data Analysis. (ed. H. H. Bock), 97-104. Elsevier, Amsterdam.

De Smedt, P., Van Meirvenne, M., Herremans, D., De Reu, J., Saey, T., Meerschman, E., Crombe, P., De Clercq, W., 2013. The 3-D reconstruction of medieval wetland reclamation through electromagnetic induction survey. Scientific Reports 3: 1517.

De Smedt, P., Van Meirvenne, M., Meerschman, E., Saey, T., Bats, M., Court-Picon, M., De Reu, J., Zwertvaegher, A., Antrop, M., Bourgeois, J., De Maeyer, P., Finke, P.A., Verniers, J., Crombé, P., 2011. Reconstructing palaeochannel morphology with a mobile multicoil electromagnetic induction sensor. Geomorphology 130: 136-141.

Kvamme, K.L., 2006. Integrating multidimensional geophysical data. Archaeological Prospection 13: 57-72.

Régionalisées. Publication N-732, Centre de Géostatistique, Ecole des Mines de Paris, Fontainebleau.

Saey, T., Simpson, D., Vermeersch, H., Cockx, L., Van Meirvenne, M., 2009. Comparing the EM38DD and Dualem-21S sensors for depth-to-clay mapping. Soil Science Society of America Journal 73: 7-12.

Saey, T., Simpson, D., Vitharana, U.W.A., Vermeersch, H., Vermang, J., Van Meirvenne, M., 2008. Reconstrucing the paleotopography beneath the loess cover with the aid of an electromagnetic induction sensor. Catena 74: 58-64.

Van Meirvenne, M., and Goovaerts, P., 2002. 'Accounting for spatial dependence in the processing of multi-temporal SAR images using factorial kriging', International Journal of Remote Sensing, 23: 371-387.

TRAINING SCHOOL 1

MICROWAVE IMAGING AND DIAGNOSTICS: THEORY, TECHNIQUES, AND APPLICATIONS

Organised by:
COST Action TU1208, COST Action TD1301,
European School of Antennas (ESoA)

Venue: Madonna di Campiglio, Italy
Dates: 24-28 March, 2014

Report by the MC Chair, Lara Pajewski

The COST Actions TU1208 "Civil Engineering Applications of Ground Penetrating Radar" and TD1301 "Development of a European-based Collaborative Network to Accelerate Technological, Clinical and Commercialisation Progress in the Area of Medical Microwave Imaging," in cooperation with the European School of Antennas (ESoA), successfully organised a Training School (TS) on "Microwave Imaging and Diagnostics: Theory, Techniques, and Applications."

The school was held in Madonna di Campiglio, a charming and elegant Italian village nestling at an altitude of 1550 metres in the stupendous valley between the Brenta Dolomites and the glaciers of Adamello and Presanella.

Electromagnetic waves can be exploited as sensing tools in a number of interesting engineering applications including Ground Penetrating Radar (GPR) prospection, antenna characterisation, biomedical diagnostics, through-the-wall imaging, and many others. The TS, after reviewing fundamental equations and main difficulties of inverse problems in high-frequency electromagnetics, focused on classical and innovative imaging techniques. Capabilities, limitations, and perspectives of both approximate and

'exact' reconstruction methods were discussed. Applicative examples were presented, with a particular focus on the topics of the organising COST Actions TU1208 and TD1301.

Coordinators of the TS were Prof Andrea Massa (ELEDIA Research Center, University of Trento, Italy, TU1208 MC Member) and Prof Tommaso Isernia (LEMMA Research Group, Mediterranea University of Reggio Calabria, TU1208 WG Member).

Teachers of the Training School were Dr Lorenzo Crocco (National Research Council, Italy, TU1208 WG Member and P4.2 Co-Leader, TD1301 MC Member), Prof Tommaso Isernia, Prof Fernando Las-Heras (Universidad Politécnica de Madrid, Spain), Dr Dominique Lesselier (SUPELEC, France, TU1208 WG Member), Prof Joe Lo-Vetri (University of Manitoba, Canada), Prof Andrea Massa, Prof Giuseppe Schettini (Roma Tre University, Italy) and Prof Alessandro Toscano (Roma Tre University, Italy).

Tutors of software exercise were Dr Giacomo Oliveri (ELEDIA Research Center, University of Trento, Italy, TU1208 WG Member), Dr Paolo Rocca (ELEDIA Research Center, University of Trento, Italy, TU1208 WG Member) and Dr Andrea Morabito (LEMMA Research Group, Mediterranea University of Reggio Calabria).

The school was attended by 39 Trainees from 14 COST Countries. There were 36% female and 64% male Trainees; 10% of the Trainees were Early-Career Investigators, all the other Trainees were PhD Students. The distribution of Trainees per Country is presented in Figure 1; it can be noted that 20% of the Trainees came from less research-intensive Countries. The Action TU1208 funded 6 TS Grants representing a contribution to cover travel, meal and accommodation expenses (50% of the grants were given to female and 50% to male Trainees); 6 further TS Grants were offered by the Action TD1301. A nice photo of a group of Trainees is reported in Figure 2.

The TS included 32.5 hours of classes (27 hours of lessons, 3.5 hours of software exercises and 2 hours of final exam), spanning over 5 days. The class scheduling is reported in the following pages.
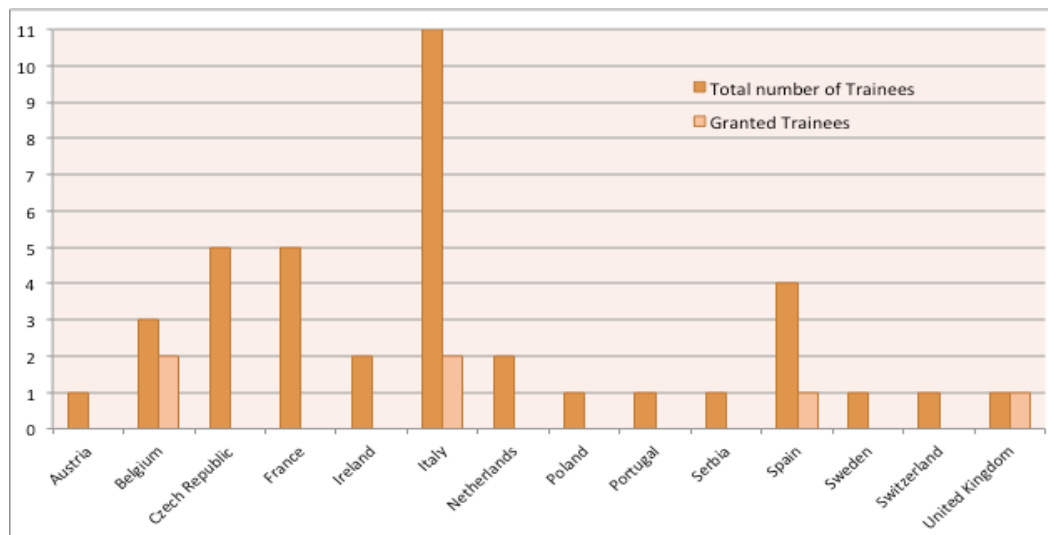
Figure 1 – Number of Trainees attending the school per Country.

CLASS SCHEDULING

Monday, 24 March 2014 - Introduction and basic theory

Time	Teacher	Activity
09:15 - 09:30		Welcome
09:30 - 11:00	A. Massa	Introduction to inverse scattering
11:00 - 11:15		Coffee break
11:15 - 12:45	A. Massa	Mathematical issues related to inverse scattering problems
12:45 - 14:30		Lunch
14:30 - 16:30	T. Isernia	Inverse source problems: radiated field properties, basic limitations, regularisation techniques
16:30 - 16:45		Coffee break
16:45 - 18:15	T. Isernia	Inverse source problems: applications to antenna characterisation, diagnostics and synthesis

79

Tuesday, 25 March 2014 - Qualitative imaging methods

Time	Teacher	Activity
08:30 - 09:30	L. Crocco	Introduction to qualitative imaging problems
09:30 - 10:30	D. Lesselier	Qualitative imaging problems: part 1
10:30 - 10:45		Coffee break
10:45 - 12:45	L. Crocco	Qualitative imaging problems: part 2
12:45 - 14:30		Lunch
14:30 - 16:30	D. Lesselier	Qualitative imaging problems: part 3
16:30 - 16:45		Coffee break
16:45 - 18:45	A. Morabito	Software exercise

Wednesday, 26 March 2014 - Quantitative imaging: approximated and complete methods

Time	Teacher	Activity
08:30 - 10:00	T. Isernia	Quantitative imaging problems: introduction
10:00 - 10:30	J. Lo-Vetri	Quantitative imaging problems (1)
10:30 - 10:45		Coffee break
10:45 - 12:45	J. Lo-Vetri	Quantitative imaging problems (2)
12:45 - 14:30		Lunch
14:30 - 16:00	A. Massa	Quantitative imaging problems (3)
16:00 - 16:15		Coffee break
16:15 - 17:15	A. Massa	Quantitative imaging problems (4)
17:15 - 18:45	G. Oliveri/ P. Rocca	Software exercise
20:30		Common dinner

Thursday, 27 March 2014 - Imaging applications

Time	Teacher	Activity
Till 14:30		Free time
14:30 - 16:30	F. Las-Heras	Case Study 1: antenna diagnostics
16:30 - 16:45		Coffee break
16:45 - 18:45	L. Crocco	Case Study 2: bio applications and COST Action TD1301

Friday, 28 March 2014 - Imaging applications, further issues and advanced topics

Time	Teacher	Activity
8:30 - 10:30	G. Schettini A. Toscano	Case Study 3: Ground Penetrating Radar applications and COST Action TU1208
10:30 - 10:45		Coffee break
10:45 - 12:45	All	Concluding remarks and future trends
12:45 - 14:30		Lunch
14:30 - 16:30	All	Final exam/test

Figure 2 – A group of Trainees attending the School.

TRAINING SCHOOL 2

FUTURE RADAR SYSTEMS: RADAR 2020

Organised by:
COST Action TU1208, European School of Antennas (ESoA),
European Microwave Association

Venue: Karlsruhe Institute of Technology, Karlsruhe, Germany
Dates: 24-28 March, 2014

Report by the MC Chair, Lara Pajewski

The COST Action TU1208 "Civil Engineering Applications of Ground Penetrating Radar," the European School of Antennas (ESoA) and the European Microwave Association (EuMA), organised a Training School on "Future Radar Systems: Radar2020."

The School was held in the Karlsruhe Institute of Technology, Karlsruhe, Germany, on May 5-9, 2014, and it covered the state of the art and new trends on radar technologies.

After an introduction to the radar basics, including propagation of electromagnetic waves, radar equation, polarimetry, analysis of Radar Cross Section (RCS) of targets and RCS measurement, the current radar types were presented, as the CW-, FMCW-, pulse-, MTI-, mono-pulse-, and UWB-radar. These lessons were complemented by the waveform and radar-parameter topics.

The core part of the course was the presentation of concepts relevant to future radars, which will be significantly different from the state of the art radars, with innovative system functions like digital beamforming, MIMO radar, intelligent signal coding (for example OFDM) and antenna array imaging for high resolution-small-size radars. Typical radar-antenna concepts for beam-forming, arrays, and phased-arrays were presented, too. Another core part of the course was represented by the introduction to some special radar applications, like automotive radar, ultra wideband radar, Ground Penetrating Radar, through-the-wall radar, and Synthetic Aperture Radar for imaging.

Coordinator of the Training School was Prof Werner Wiesbeck (Karlsruhe Institute of Technology, Germany, TU1208 WG Member). Trainers were Prof Werner Wiesbeck, Prof Thomas Zwick (Karlsruhe Institute of Technology, Germany), Prof Alexander Yarovoy (Delft University of Technology, The Netherlands, TU1208 WG Member), and Prof Marwan Younis (Karlsruhe Institute of Technology, Germany). Moreover, Dr Lara Pajewski (Roma Tre University, Italy, TU1208 Chair) attended part of the school and gave a presentation to introduce the COST framework and present the COST Action TU1208.

The number of Trainees attending the school per Country is reported in Figure 1. The total number of Trainees was 16, from 7 COST Countries; the percentage of female Trainees was 18.75%; only 6.25% of the Trainees came from less research-intensive Countries. The Action TU1208 offered 4 TS Grants to Trainees attending the School, as a contribution to cover travel, meal and accommodation expenses; the percentage of grants given to female Trainees was 25%.

A photo of the Trainees is shown in Figure 2, whereas in the next pages the class scheduling is reported.
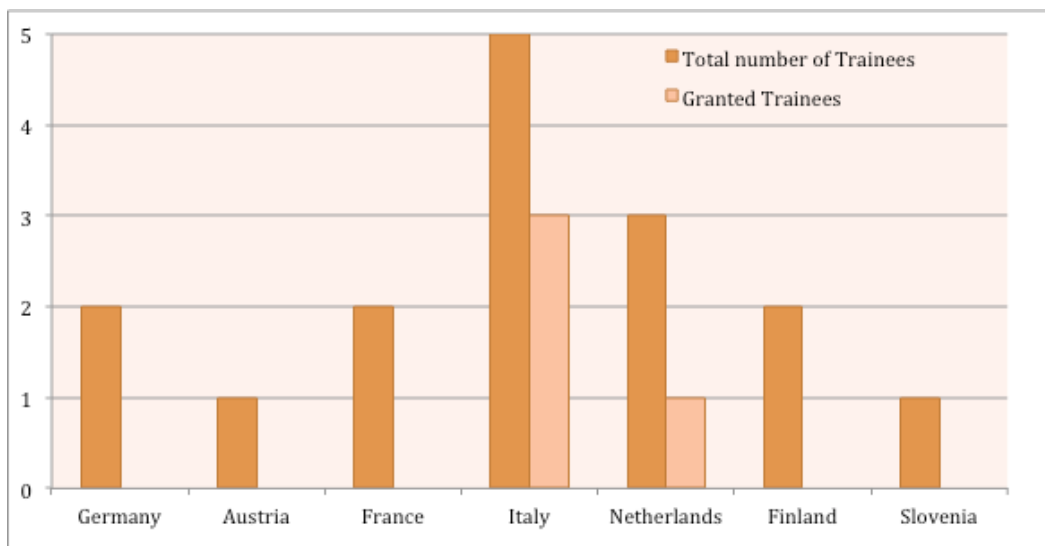
Figure 1 – Number of Trainees attending the school per Country.

CLASS SCHEDULING

Monday, 5 May 2014 - Introduction and basic theory

Time	Teacher	Activity
08:30 - 10:00		Registration and welcome.
10:00 - 10:30		Break
10:30 - 12:00	W. Wiesbeck	Introduction, overview, radar history.
12:00 - 13:30		Lunch
13:30 - 15:00	W. Wiesbeck	Propagation phenomena. Polarimetry.
15:00 - 15:30		Break
15:30 - 17:00	W. Wiesbeck	Radar equation. Resolution. Accuracy.
17:00 - 18:00	W. Wiesbeck	Exercise. Discussion.

Tuesday, 6 May 2014 - Basic theory and radar types

Time	Teacher	Activity
08:30 - 10:00	W. Wiesbeck	RCS definition. RCS of targets.
10:00 - 10:30		Break
10:30 - 12:00	W. Wiesbeck	Radar types. Pulse radar.
12:00 - 13:30		Lunch
13:30 - 15:00	T. Zwick	CW and FM-CW radars. Coding.
15:00 - 15:30		Break
15:30 - 17:00	T. Zwick	Automotive radar. Virtual drive.
17:00 - 18:00	T. Zwick	Exercise. Discussion.

Wednesday, 7 May 2014 - Future radar systems and Laboratory

Time	Teacher	Activity
08:30 - 10:00	W. Wiesbeck	Future radar systems. OFDM radar.
10:00 - 10:30		Break
10:30 - 12:00	W. Wiesbeck	DSSS coding. Digital beamforming.
12:00 - 13:30		Lunch
13:30 - 15:00	W. Wiesbeck	MIMO radar. Array imaging.
15:00 - 15:30		Break
15:30 - 17:30	Daimler, IHE	Automotive radar demonstration.
19:00		Common dinner

Thursday, 8 May 2014 - GPR and SAR

Time	Teacher	Activity
8:30 - 10:00	A. Yarovoy	UWB radar basics.
10:00 - 10:30		Break
10:30 - 12:00	A. Yarovoy	GPR and through-the-wall radar.
12:00 - 12:30	L. Pajewski	COST Action TU1208
12:30 - 14:00		Lunch
14:00 - 15:30	M. Younis	SAR principles. SAR processing.
15:30 - 16:00		Break
16:00 - 17:30	M. Younis	SAR performance parameters. SAR modes.
17:30 - 18:00	M. Younis	Exercise. Discussion.

Friday, 9 May 2014 - SAR and final test

Time	Teacher	Activity
8:30 - 10:00	M. Younis	SAR Systems. SAR DBF.
10:00 - 10:30		Lunch
10:30 - 11:30	All	Discussion.
11:30 - 12:30		Lunch
12:30 - 14:30	All	Final exam

Figure 2 – Trainees and Prof Werner Wiesbeck in front of the
monument devoted to Heinrich Hertz.

TABLE OF CONTENTS

STSM 2 – "The preservation of the Tholos Tomb of Acharnon"

Visiting Scientist: *Sonia Santos Assuncao,* Host: *Klisthenis Dimitriadis*

STSM 3 – "Numerical modelling of Ground Penetrating Radar antennas"

Visiting scientist: *Iraklis Giannakis,* Host: *Lara Pajewski*

STSM 4 – "Reconstructing prehistoric environments at Stonehenge with multiple electromagnetic survey methods"

Visiting scientist: *Philippe De Smedt,* Host: *Immo Trinks*

COST - European Cooperation in Science and Technology is an intergovernmental framework aimed at facilitating the collaboration and networking of scientists and researchers at European level. It was established in 1971 by 19 member countries and currently includes 35 member countries across Europe, and Israel as a cooperating state.

COST funds pan-European, bottom-up networks of scientists and researchers across all science and technology fields. These networks, called 'COST Actions', promote international coordination of nationally-funded research. By fostering the networking of researchers at an international level, COST enables break-through scientific developments leading to new concepts and products, thereby contributing to strengthening Europe's research and innovation capacities.

COST's mission focuses in particular on: building capacity by connecting high quality scientific communities throughout Europe and worldwide; providing networking opportunities for early career investigators; increasing the impact of research on policy makers, regulatory bodies and national decision makers as well as the private sector.

Through its inclusiveness, COST supports the integration of research communities, leverages national research investments and addresses issues of global relevance. Every year thousands of European scientists benefit from being involved in COST Actions, allowing the pooling of national research funding to achieve common goals.

As a precursor of advanced multidisciplinary research, COST anticipates and complements the activities of EU Framework Programmes, constituting a "bridge" towards the scientific communities of emerging countries. In particular, COST Actions are also open to participation by non-European scientists coming from neighbour countries (for example Albania, Algeria, Armenia, Azerbaijan, Belarus, Egypt, Georgia, Jordan, Lebanon, Libya, Moldova, Montenegro, Morocco, the Palestinian Authority, Russia, Syria, Tunisia and Ukraine) and from a number of international partner countries.

COST's budget for networking activities has traditionally been provided by successive EU RTD Framework Programmes. COST is currently executed by the European Science Foundation (ESF) through the COST Office on a mandate by the European Commission, and the framework is governed by a Committee of Senior Officials (CSO) representing all its 35 member countries.

More information about COST is available at www.cost.eu.

The scientific activities of the COST Action TU1208 are carried out within four Working Groups (WGs). The effectiveness of this scheme will be checked after the first year of activities and will eventually be modified, considering the actual number of active participants in each WG. The structure of each WG will always be kept as flexible as possible, in order to enable new participants to join. All the participants, when joining the Action, are invited to provide basic information on their experience, interests, and current research projects, as well as WGs and Projects preferences. Each participant can belong to two WGs and an arbitrary number of projects within the chosen WGs.

The four TU1208 WGs are: WG1 – Novel GPR instrumentation; WG2 – GPR surveying of pavements, bridges, tunnels and buildings; underground utility and void sensing; WG3 – EM methods for near-field scattering problems by buried structures and data processing techniques; WG4 – Different applications of GPR and other NDT technologies in civil engineering. The WG meetings constitute an opportunity to present activities, results and plans for the future. Between meetings, the WG members regularly interact.

COST ACTION TU1208

CIVIL ENGINEERING APPLICATIONS OF GROUND PENETRATING RADAR

Short-Term Scientific Missions and Training Schools - Year 1

The COST Action TU1208 focuses on the exchange of scientific-technical knowledge and experience of Ground Penetrating Radar (GPR) techniques in Civil Engineering (CE). The project is being developed within the frame of a unique approach based on the integrated contribution of University researchers, software developers, geophysics experts, Non-Destructive Testing equipment designers and producers, end users from private companies and public agencies. In this interdisciplinary Action, advantages and limitations of GPR will be highlighted leading to the identification of gaps in knowledge and technology. Protocols and guidelines for EU Standards will be developed, for effective application of GPR in CE. A novel GPR will be designed and realized: a multi-static system, with dedicated software and calibration procedures, able to construct real-time lane 3D high resolution images of investigated areas. Advanced electromagnetic-scattering and data-processing techniques will be developed. The understanding of relationships between geophysical parameters and CE needs will be improved. Freeware software will be released, for inspection and monitoring of structures and infrastructures, buried-object localization, shape reconstruction and estimation of useful parameters. A high level training program will be organized. Mobility of early career researchers will be encouraged. The project has already received the interest of key end users and excellent EU Institutions.

www.GPRadar.eu

www.cost.eu/domains_actions/tud/Actions/TU1208

This publication is supported by COST